Synthesis and Structural-Bonding Analysis of the 50/49/48-Electron Triangular Metal $[Co_3(\eta^5\text{-}C_5H_4Me)_3(\mu_3\text{-}S)_2]^n$ Series (n = 0, 1+, 2+): Singlet-Triplet Solution Equilibrium of the Solid-State Diamagnetic 50-Electron $Co_3(\eta^5\text{-}C_5H_4Me)_3(\mu_3\text{-}S)_2$ Cluster

Curtis R. Pulliam,[1a,b] James B. Thoden,[1a] Angelica M. Stacy,[1c] Brock Spencer,[1d] Mark H. Englert,[1a,e] and Lawrence F. Dahl*,[1a]

Contribution from the Departments of Chemistry, University of Wisconsin—Madison, Madison, Wisconsin 53706, University of California, Berkeley, California 94720, and Beloit College, Beloit, Wisconsin 53511. *Received February 11, 1991*

Abstract: The isolation and stereochemical characterization of the 50/49/48-electron triangular metal members (n = 0, 1+, 2+) of the $[Co_3Cp'_3(\mu_3\text{-}S)_2]^n$ series (Cp' = η^5-C_5H_4Me) are reported; their solid-state and solution properties are compared with those of the corresponding members of the $[Co_3Cp_3(\mu_3\text{-}S)_2]^n$ series (Cp = η^5-C_5H_5). Noncylindrical Cp' ligands were substituted for cylindrical Cp ligands in order to reduce the likelihood that the neutral 50-electron Cp'-containing **1** would have crystallographically imposed C_{3h}-3/m site symmetry (i.e., an averaged structure) as previously found in $Co_3Cp_3(\mu_3\text{-}S)_2$ (**2**); the replacement of Cp with Cp' ligands results in different *solid-state* Co_3S_2 core geometries and concomitantly different electronic configurations at room temperature for the 50-electron neutral parents as well as for their corresponding 49-electron monocations. However, both neutral clusters exhibit similar temperature-dependent ^{1}H NMR solution behavior involving a singlet-triplet spin equilibrium that shifts toward the singlet state at lower temperatures. The neutral parents (**1**, **2**) of both series were prepared (in 15-20% yields) by a new, convenient synthetic route involving reactions of $Co(\eta^5\text{-}C_5H_{5-x}Me_x)(CO)_2$ (x = 0, 1) with neat CS_2. Oxidations of **1** with either $AgPF_6$ or $AgSbF_6$ produced the 49-electron $\mathbf{1}^+$ and 48-electron $\mathbf{1}^{2+}$, which were isolated as their $[PF_6]^-$ or $[SbF_6]^-$ salts. Cyclic voltammetric measurements of **1**, $\mathbf{1}^+$, and $\mathbf{1}^{2+}$ revealed self-consistent electrochemical behavior, which for **1** involves one reversible reduction to form $\mathbf{1}^-$ and two reversible oxidations to form $\mathbf{1}^+$ and $\mathbf{1}^{2+}$. **1**, $\mathbf{1}^+[PF_6]^-$, and $\mathbf{1}^{2+}[SbF_6]^-_2$ were characterized by single-crystal X-ray diffraction and **1** and $\mathbf{1}^+[PF_6]^-$ by EPR and magnetic susceptibility studies. The X-ray crystallographic analysis of **1** was performed at room temperature in order to determine the geometrical effects of the two antibonding electrons that are in excess of the 48 electrons necessary for a complete metal-metal-bonded M_3S_2 system. The geometrically analogous Co_3S_2 cores of the two crystallographically independent molecules of **1** closely conform to C_{2v}-2-mm geometry with the isosceles cobalt triangle possessing one nonbonding edge of 3.19 Å (av) and two electron-pair bonding edges of 2.48 Å (av). Solid-state magnetic susceptibility measurements revealed that **1** is diamagnetic over the entire temperature range from 6 to 280 K. These observations provide convincing evidence that the two spin-paired antibonding electrons in **1** must be localized along the nonbonding Co-Co edge in a nondegenerate MO, which is antisymmetric with respect to the vertical mirror plane bisecting the long edge of the metal triangle. In sharp contrast, the previously characterized $Co_3Cp_3(\mu_3\text{-}S)_2$ (**2**) has two unpaired electrons at room temperature in accordance with an instantaneous equilateral metal triangle. A ^{1}H NMR investigation of **1** revealed dramatic temperature-dependent shifts of the three distinct Cp' proton resonances from paramagnetic-induced values at 301 K toward their diamagnetic-limiting values at 168 K; the isotropic shift behavior of the two Cp' ring-proton resonances with decreasing temperature is similar to that previously observed for the Cp proton resonance in **2**. These variable-temperature ^{1}H NMR data were analyzed on the basis of a singlet-triplet equilibrium in solution involving a triplet spin-state species with a presumed D_{3h} Co_3S_2 core geometry and a singlet spin-state species with a distorted C_{2v} Co_3S_2 core geometry. The temperature-dependent isotropic shift data for the three proton resonances of **1** and for the one proton resonance of **2** were found to give excellent, self-consistent least-squares fits to a generalized form of the contact shift equation. A room-temperature X-ray crystallographic analysis of $\mathbf{1}^+[PF_6]^-$ showed that the removal of one of the two antibonding electrons in **1** results primarily in the nonbonding edge of the C_{2v} cobalt triangle decreasing in length by 0.32 Å to a "net one-electron" bonding edge (2.873 (1) Å), which is 0.38 Å longer than the two unaltered electron-pair bonding edges (2.486 (1), 2.495 (1) Å). The inversion of this isosceles metal triangle in $\mathbf{1}^+$ from that of the Jahn-Teller distorted C_{2v} Co_3S_2 geometry in $\mathbf{2}^+$, which in both the $[SbF_6]^-$ and $[I]^-$ salts possesses one short (2.50 Å) and two longer (2.65 Å) bonding edges, is attributed to the different electronic ground states of their neutral precursors. Formation of the 48-electron $\mathbf{1}^{2+}$ from $\mathbf{1}^+$ by removal of the second antibonding electron results in a further 0.35-Å decrease of the longer Co-Co distance in $\mathbf{1}^+$ to give a pseudoequilateral metal triangle in $\mathbf{1}^{2+}$ with three electron-pair metal-metal bonds of 2.52 Å (av). The analogous mean Co-Co distances in the 50-electron **1** (2.72 Å) and **2** (2.69 Å) are 0.10 Å longer than those in the corresponding 49-electron monocations of $\mathbf{1}^+[PF_6]^-$ (2.62 Å), $\mathbf{2}^+[SbF_6]^-$ (2.60 Å), and $\mathbf{2}^+[I]^-$ (2.59 Å), which in turn are 0.10 Å longer than that in the 48-electron $\mathbf{1}^{2+}[SbF_6]^-_2$ (2.52 Å). This correlation of metal-metal distances with the number of "excess" trimetal-antibonding electrons in a localized valence-bond scheme provides persuasive bond length support for the validity of the electron-counting formalism, which assumes that the HOMOs for these 49- and 50-electron triangular metal clusters possess *trimetal-antibonding* orbital character. A comparison of these structural-bonding analyses with the conclusions from previous Fenske-Hall MO calculations is given. That these theoretical MO interpretations do not relate the electronic-geometrical changes with the orbital nature of direct metal-metal interactions (which are relatively weak and not localized) in these electron-rich triangular metal clusters is attributed largely to the neglect (or underestimation) of the importance of the more diffuse Co 4s and 4p_z AOs; these minor trimetal-antibonding contributions to the frontier e' HOMOs (under assumed D_{3h} symmetry) are presumed to dominate over the major trimetal-bonding in-plane Co 3d_{xz} contributions due to much better orbital overlap at long Co-Co distances.

Introduction

An extensive part of our systematic research on transition-metal cluster chemistry has involved the structural effects generated by reversible electron-transfer processes in small metal cluster systems.[2] The study of structural-redox relationships has important theoretical implications with regard to the bonding description of transition metal-main group clusters whose metal cores function

0002-7863/91/1513-7398$02.50/0

as electron reservoirs. There is particular interest in elucidating the mechanisms of electron-transfer reactions in which paramagnetic intermediates are formed.

In connection with an examination of electron-induced variations in geometry that occur in electron-rich bicapped tricobalt and trinickel clusters upon variation in ligation about the metal cluster cores, we describe here how the substitution of noncylindrical Cp′ ligands for cylindrical Cp ligands causes a change at room temperature of the solid-state architecture and electronic configuration of Co_3S_2 cores not only between the neutral parents but also between the oxidized monocations.

The neutral $Co_3Cp_3(\mu_3\text{-}S)_2$ (**2**) has been previously studied and stereophysically characterized.[3-6] This unusual 50-electron triangular metal cluster, which possesses two electrons more than the 48 needed for a metal triangle with three single bonds, and the corresponding 48-electron $Co_3Cp_3(\mu_3\text{-}CO)(\mu_3\text{-}S)$ were first prepared and isolated by Otsuka et al.[3] from the reaction of $CoCp(CO)_2$ with bis(*tert*-butylimido)sulfur. Independent single-crystal X-ray diffraction studies[5-10] at room temperature established that **2** is isostructural with other known $M_3(\eta^5\text{-}C_5R_5)_3(\mu_3\text{-}X)_2$ species (R = H, Me)[9,11] and crystallizes with imposed C_{3h}-3/*m* site symmetry; furthermore, each Cp ring is presumed to possess a 2-fold orientational disorder such that the crystallographic site symmetry in each molecule is increased to D_{3h}-$\bar{6}2m$ This raises the possibility that the observed D_{3h} Co_3S_2 core geometry in **2** is the result of a 3-fold rotational averaging of molecules of actual C_{2v} symmetry. The true Co_3S_2 core geometry of this molecule plays a crucial role in the analysis of the nature of the frontier orbitals.

Solid-state magnetic susceptibility measurements[3,5] showed that **2** exhibits a paramagnetism at room temperature characteristic of two unpaired electrons. Independent investigations of the solid-state magnetic properties of **2** as a function of temperature gave similar results;[3,5] bulk susceptibility data measured in our laboratories from 98 to 340 K exhibited Curie–Weiss behavior from 340 to 196 K where an abrupt discontinuity occurs such that at 166 K the molar susceptibility has dropped sharply to approximately half of its maximum value (at T_N = 196 K).[5,12] From variable-temperature heat capacity measurements of **2**, Sorai et al.[4] discovered a phase transition at 192.5 (1) K with transition enthalpy and entropy values of 5.25 kJ/mol and 28.9 J/mol·K, respectively. The complementary solid-state magnetic and thermal data provided conclusive evidence that this phase transition must be associated with a change in spin state involving an interconversion from a singlet state at low temperatures to a triplet state at high temperatures. The unusually large entropy value at this phase transition was attributed by Sorai et al.[4] to the sum of a magnetic contribution arising from the singlet to triplet excitation of electrons and an order–disorder configurational contribution due to a cooperative coupling arising from the gearlike rotational motion of the reorientating Cp rings and molecular electronic states.

Proton NMR spectra of **2** were found to exhibit a dramatic temperature dependence of the cyclopentadienyl proton resonance, which changes from a paramagnetic-induced broad singlet around δ −0.48 at 51 °C to a sharp, normal diamagnetic singlet of δ 4.67 at −100 °C.[3,5] These variable-temperature ^{1}H NMR data were analyzed on the basis of a singlet–triplet solution equilibrium that shifts to the singlet state at lower temperatures.[5]

Sorai et al.[4] proposed that the magnetic behavior of **2** can only be explained by a level crossing of two close-lying MOs, a nondegenerate a_2' and a doubly degenerate e′ (under assumed D_{3h} symmetry). Unfortunately, their proposed temperature-dependent energy scheme was flawed by the assignment of an incorrect number of electrons (i.e., four instead of two) to the frontier a_2' and e′ MOs. Frisch and Dahl[5] likewise rationalized the ^{1}H NMR singlet–triplet data in terms of a crossover of the a_2' and e′ energy levels, with the a_2' level lower and doubly occupied at low temperatures (in accordance with the singlet state) and the e′ levels lower and doubly occupied at high temperatures (in accordance with the triplet state). In harmony with Sorai et al.,[4] Frisch and Dahl[5] speculated that this change in electronic structure may be primarily a consequence of the metal–Cp interactions due to a vibronic effect caused by more restricted Cp motion at lower temperatures.

An alternative electronic model for **2** was subsequently put forth by Rives, You, and Fenske.[13] They used the nonparameterized Fenske–Hall model[14] to do approximate molecular orbital calculations on **2** and on the diamagnetic 50-electron $Fe_3(CO)_9(\mu_3\text{-}S)_2$,[15-17] which in the solid state is composed of a highly distorted isosceles iron triangle with two electron-pair bonding sides (2.60 Å (av)) and one nonbonding side (3.37 Å). Since their results revealed that the a_2' and e′ levels are very close in both the Co_3S_2 and Fe_3S_2 clusters, they then resorted to comparisons with experimental data to rationalize the electronic structures of these compounds. The observed C_{2v} Fe_3S_2 core geometry was attributed to the two electrons under D_{3h} symmetry being spin-paired in the e′ MOs, giving rise to a singlet ^{1}E′ state, which is distorted to the observed C_{2v} geometry via a Jahn–Teller mechanism. Since both the a_2' and one of the e′ MOs under D_{3h} symmetry transform as the b_1 representation under the observed C_{2v} symmetry of the molecule, mixing of the two orbitals may occur. Rives, You, and Fenske[13] suggested that the HOMO of $Fe_3(CO)_9(\mu_3\text{-}S)_2$ is 40% a_2' and 60% e′, which they described as

(1) (a) University of Wisconsin—Madison. (b) Present address: Department of Chemistry, Utica College of Syracuse University, Utica, NY 13502. (c) University of California—Berkeley. (d) Beloit College. (e) Present address: USG Corp., Libertyville, IL 60048.

(2) (a) For a compilation of older references, see: Kharas, K. C. C.; Dahl, L. F. Ligand-Stabilized Metal Clusters: Structure, Bonding, Fluxionality, and the Metallic State. *Adv. Chem. Phys.* **1988**, *70* (part 2), 1–43 (ref 39). (b) Kubat-Martin, K. A.; Barr, M. E.; Spencer, B.; Dahl, L. F. *Organometallics* **1987**, *6*, 2570–2579. (c) Kubat-Martin, K. A.; Spencer, B.; Dahl, L. F. *Organometallics* **1987**, *6*, 2580–2587. (d) Ziebarth, M. S.; Dahl, L. F. *J. Am. Chem. Soc.* **1990**, *112*, 2411–2418.

(3) (a) Otsuka, S.; Nakamura, A.; Yoshida, T. *Inorg. Chem.* **1968**, *7*, 261–265. (b) Otsuka, S.; Nakamura, A.; Yoshida, T. *Justus Liebigs Ann. Chem.* **1968**, *719*, 54–60.

(4) Sorai, M.; Kosaki, A.; Suga, H.; Seki, S.; Yoshida, T.; Otsuka, S. *Bull. Chem. Soc. Jpn.* **1971**, *44*, 2364–2371.

(5) (a) Frisch, P. D.; Dahl, L. F. *J. Am. Chem. Soc.* **1972**, *94*, 5082–5084. (b) Frisch, P. D. Ph.D. Thesis, University of Wisconsin—Madison, Madison, WI, 1972.

(6) Kamijo, N.; Watanabe, T. *Acta Crystallogr.* **1979**, *B35*, 2537–2542.

(7) The crystal structure of the room-temperature phase of **2** was complicated by a twinning of the hexagonal crystals; its structure was solved independently by Frisch and Dahl[5] and by Kamijo and Watanabe[6] via the application of the twinning model originally developed by Wei[8] and utilized in our laboratories to unravel and refine the crystal structures of the isostructural 53-electron $Ni_3Cp_3(\mu_3\text{-}S)_2$,[9] the 48-electron $Co_3Cp_3(\mu_3\text{-}CO)(\mu_3\text{-}O)$,[10] and the 48-electron $Co_3Cp_3(\mu_3\text{-}CO)(\mu_3\text{-}S)$.[3,5] The two structural determinations gave experimentally equivalent molecular parameters for **2** including values of 2.687 (3) and 2.691 (4) Å for the independent Co–Co distance for the Co_3S_2 core of crystallographic C_{3h}-3/*m* site symmetry.

(8) (a) Wei, C. H.; Wilkes, G. R.; Dahl, L. F. *J. Am. Chem. Soc.* **1967**, *89*, 4792–4793. (b) Wei, C. H. *Inorg. Chem.* **1969**, *8*, 2384–2397.

(9) Vahrenkamp, H.; Uchtman, V. A.; Dahl, L. F. *J. Am. Chem. Soc.* **1968**, *90*, 3272–3273.

(10) Uchtman, V. A.; Dahl, L. F. *J. Am. Chem. Soc.* **1969**, *91*, 3763–3769.

(11) (a) $Ni_3Cp_3(\mu_3\text{-}CO)_2$: (i) Hock, A. A.; Mills, O. S. In *Advances in the Chemistry of Coordination Compounds*; Kirschner, S., Ed.; Macmillan: New York, 1961; pp 640–648. (ii) Byers, L. R.; Uchtman, V. A.; Dahl, L. F. *J. Am. Chem. Soc.* **1981**, *103*, 1942–1951. (b) $Ni_3Cp^*_3(\mu_3\text{-}CO)_2$: Maj, J. A.; Rae, A. D.; Dahl, L. F. *J. Am. Chem. Soc.* **1982**, *104*, 3054–3063. (c) $Co_3Cp_3(\mu_3\text{-}NO)_2$: Kubat-Martin, K. A.; Rae, A. D.; Dahl, L. F. *Organometallics* **1985**, *4*, 2221–2223. (d) $Co_3Cp_3(\mu_3\text{-}CO)_2$: Barnes, C. E.; Orvis, J. A.; Staley, D. L.; Rheingold, A. L.; Johnson, D. C. *J. Am. Chem. Soc.* **1989**, *111*, 4992–4994. (e) $Co_3Cp^*_3(\mu_3\text{-}CO)_2$: Olson, W. L.; Stacy, A. M.; Dahl, L. F. *J. Am. Chem. Soc.* **1986**, *108*, 7646–7656.

(12) The effective magnetic moment, calculated from $\mu_{eff} = 2.828(\chi_M T)^{1/2}$, decreases slightly in a linear manner from 2.83 μ_B at 340 K to 2.68 μ_B at 197.7 K; it then undergoes a sharp discontinuity at 196 K, below which the magnetic moment decreases exponentially such that it has a value of 0.93 μ_B at 98 K.[5]

(13) Rives, A. B.; You, X.-Z.; Fenske, R. F. *Inorg. Chem.* **1982**, *21*, 2286–2294.

(14) Hall, M. B.; Fenske, R. F. *Inorg. Chem.* **1972**, *11*, 768–775.

(15) Wei, C. H.; Dahl, L. F. *Inorg. Chem.* **1965**, *4*, 493–499.

(16) A corresponding 50-electron disulfur-capped diiron–cobalt cluster, $(OC)_6Fe_2Co(\eta^5\text{-}C_5H_4CO_2Me)(\mu_3\text{-}S)_2$, containing a nonbonding Fe–Fe distance (3.369 (1) Å) and two electron-pair bonding Fe–Co distances (2.521 (1), 2.541 (1) Å) was recently prepared and structurally characterized from an X-ray diffraction study.[17]

(17) Wakatsuki, Y.; Yamazaki, H.; Cheng, G. *J. Organomet. Chem.* **1988**, *347*, 151–156.

$^1E'(a_2'e')$. They predicted that the diamagnetic, low-temperature form of **2** would be similar to the electronically equivalent $Fe_3(CO)_9(\mu_3\text{-}S)_2$ and thus would possess a C_{2v} Co_3S_2 core geometry with a $^1E'(a_2'e')$ ground state.[18] At higher temperatures they suggested that the stabilization provided via singlet spin coupling would be overcome and the $^3E'$ state would become populated. They further speculated that the apparent D_{3h} point group imposed for the Co_3S_2 core geometry of **2** at room temperature is an artifact and that this molecule is likely distorted to some extent from 3-fold rotational symmetry.

The theoretical-based interpretations by Rives et al.[13] of the orbital nature of the direct metal–metal interactions in **2**, its monocation $\mathbf{2}^+$, and related trimetal clusters are not compatible with our previous correlations[5,9,11b] of the metal–metal distances in the 49-, 50-, and 53-electron systems with the number of antibonding valence electrons within their M_3X_2 cores (i.e., in particular their designation of the e′ MOs as trimetal-bonding instead of trimetal-antibonding). Hence, we decided to perform an operational test of these structural-bonding models for the 50/49/48-electron $[Co_3Cp_3(\mu_3\text{-}S)_2]^n$ series (n = 0, 1+, 2+) by preparing the corresponding $[Co_3Cp'_3(\mu_3\text{-}S)_2]^n$ series for comparative stereophysical analysis. We hoped that the methyl-substituted Cp′ rings would (1) permit **1** to crystallize without imposed C_{3h} symmetry, thereby allowing an unambiguous analysis of its molecular geometry at room temperature; (2) decrease the dynamic rotational ring motions in the solid state relative to those of the Cp rings in **2** so that the presumed diamagnetic isomer of **1** would be stabilized at a higher temperature; and (3) allow a better probe of the nature of the solution singlet–triplet equilibrium. We expected there would be three separate proton NMR resonances (i.e., one methyl and two pairs of ring proton signals) for equivalent Cp′ ligands under localized C_{2v} ring symmetry.

Presented herein are the details of a convenient preparation of $Co_3Cp'_3(\mu_3\text{-}S)_2$ (**1**), its electrochemical behavior, its crystal structure, and its solid-state and solution magnetic properties. An analysis of the observed temperature-dependent equilibrium between the singlet and triplet spin states in solution is presented. We have also chemically oxidized **1** and isolated salts of the monocation ($\mathbf{1}^+$) and dication ($\mathbf{1}^{2+}$) for X-ray crystallographic studies. We propose an alternative viewpoint that the structural changes occurring upon oxidation of 50-electron **1** or **2** can be accounted for by the minor s–p trimetal-antibonding orbital components of the e′ HOMOs (under assumed D_{3h} symmetry) instead of by major d_{xz} trimetal-bonding orbital components.

Recently, Wakatsuki et al.[19] reported the preparation and room-temperature X-ray diffraction, variable-temperature solid-state magnetic susceptibility, and variable-temperature solution ^1H NMR analyses of the 50-electron $Co_3(\eta^5\text{-}C_5H_4CO_2Me)_3(\mu_3\text{-}S)(\mu_3\text{-}N^tBu)$ along with the preparation and variable-temperature ^1H NMR investigation of the corresponding 50-electron $Co_3(\eta^5\text{-}C_5H_4CO_2Me)_3(\mu_3\text{-}S)_2$. Their results will be discussed as they relate to this reported study.

Experimental Section

General Techniques and Materials. Unless otherwise stated, all reactions and manipulations were performed with Schlenk-type apparatus under an atmosphere of prepurified nitrogen, either with a preparative vacuum-line or within a Vacuum Atmospheres drybox. The following solvents were freshly distilled from the indicated drying agents and saturated with N_2 immediately prior to use: acetonitrile (CaH_2), benzene (CaH_2), carbon disulfide (P_2O_5), and dichloromethane (P_2O_5). Chloroform-d_1 was dried over molecular sieves, frozen and degassed three times, and vacuum-distilled before use. Dichloromethane-d_2 (Aldrich Gold Label) was used, as received, from freshly opened ampules. $CoCp'(CO)_2$ was analogously prepared by the method described[20] for the preparation of $CoCp(CO)_2$. All other reagents were purchased from major chemical suppliers and used without further purification. Infrared spectra were recorded on a Beckman Model 4240 spectrophotometer. Proton NMR spectra were recorded on a Bruker WP-270 FT-NMR spectrometer.

Cyclic and linear sweep voltammetric studies were performed with a BAS-100 electrochemical analyzer in conjunction with a PAR electrochemical cell. All measurements were made inside a drybox under an atmosphere of recirculating purified nitrogen; details are given elsewhere.[21] An *iR* compensation for solution resistance[22] was made before the current–voltage curves were obtained. An electron-transfer process was assumed to be chemically reversible when the ratio of the peak currents for the reduction and oxidation waves (I_c/I_a) was approximately unity over a scan rate range of 50–500 mV/s.

$Co_3Cp'_3(\mu_3\text{-}S)_2$ (1). (a) Preparation. $CoCp'(CO)_2$ (5.0 mL) was refluxed under a blanket of N_2 in CS_2 (150 mL) until all the starting material had reacted, as shown after approximately 48 h by the total disappearance of carbonyl absorption bands in the spectra of the IR-monitored reaction mixture. The CS_2 was removed under vacuum and the residue exhaustively extracted with 50-mL portions of a 1:1 (v/v) hexane–benzene mixture. The extracts were combined, reduced in volume, and loaded onto a chromatographic column containing oxygen-free alumina (activity grade 3, Brockman 80–200 mesh, Fischer Scientific) packed with hexane and maintained under nitrogen. Elution with 10% benzene in hexane led to removal of the first brown band, which was sometimes preceded by a small blue band. This brown band yielded, after solvent removal, crystals of the desired $Co_3Cp'_3(\mu_3\text{-}S)_2$ (**1**) in 15–20% yield.[23,24]

(b) Characterization. (1) Properties. This compound is soluble in most organic solvents, both polar and nonpolar. A mid-IR spectrum of **1** did not exhibit any intense identifying bands.

(2) Electrochemical Data. Three chemically reversible processes (viz., one reduction and two oxidation couples) are displayed in a cyclic voltammogram of **1** in CH_2Cl_2 at a scan rate of 200 mV/s (Figure 1). The first oxidation couple, $0 \rightarrow 1+$, occurs at $E_{1/2} = -0.26$ V (all voltage measurements vs SCE) with a peak to peak separation (ΔE_p) of 64 mV. The second oxidation couple, $1+ \rightarrow 2+$, has a measured $E_{1/2} = +0.52$ V and $\Delta E_p = 76$ mV. The $0 \rightarrow 1-$ reduction couple has an $E_{1/2} = -1.31$ V and $\Delta E_p = 74$ mV. The half-wave potentials and peak to peak separations of **1** in CH_3CN at 200 mV/s are as follows: $0 \rightarrow 1+$, $E_{1/2} = -0.35$ V, $\Delta E_p = 63$ mV; $1+ \rightarrow 2+$, $E_{1/2} = 0.36$ V, $\Delta E_p = 66$ mV; $0 \rightarrow 1-$, $E_{1/2} = -1.32$ V, $\Delta E_p = 79$ mV. Cyclic voltammetric measurements reported by Madach and Vahrenkamp[25] for $Co_3Cp_3(\mu_3\text{-}S)_2$ (**2**) in benzonitrile analogously showed one reversible 1-electron reduction and two reversible 1-electron oxidation couples.

(3) Solid-State Magnetic Susceptibility Data. Variable-temperature and field-dependent magnetic susceptibility measurements of **1** were performed from 6 to 280 K in fields of 5 and 40 kG with a SHE series 900 SQUID magnetometer (University of California—Berkeley). The sample was loaded into a Kel-f container in a Vacuum Atmospheres glovebox and sealed under dry argon. The magnetic susceptibilities were corrected for the diamagnetism due to the Kel-f container. $Co_3Cp'_3(\mu_3\text{-}S)_2$ is diamagnetic over the entire temperature range, and the susceptibility is nearly temperature-independent (Figure 2). In a field of 40 kG, the molar susceptibility changes from -0.308×10^{-3} mol^{-1} at 6 K to -0.135×10^{-3} mol^{-1} at 280 K. This small increase in susceptibility with increasing temperature is probably an artifact due to a small error in the container calibration. The observed value for the diamagnetism agrees well with the estimated value of -0.248×10^{-3} mol^{-1} ($C_5H_4Me^-$, -57.71×10^{-6}; Co^+, -15.0×10^{-6}; S^0, -15.0×10^{-6}).[26] In a field of 5 kG, the susceptibility is -0.275×10^{-3} mol^{-1}, essentially identical with that observed in a field of 40 kG; the field independence of the measured susceptibility shows that the sample is free of ferromagnetic impurities.

(18) An X-ray diffraction study at 130 (5) K was carried out by Kamijo and Watanabe[6] on the low-temperature phase of **2**. A twinnal hexagonal superstructure ($P6_1$ with Z = 18) of the room-temperature twinned structure was found. The structural analysis was based on the assumption that the three crystallographically independent molecules within the same plane (i.e., with identical atomic z coordinates) are related to one another by a noncrystallographic 3-fold axis. The Co_3S_2 core of C_1-1 site symmetry for the resulting independent molecule was determined from a bounded Fourier projection to be distorted from D_{3h} symmetry with one longer Co–Co distance of 2.76 Å and two shorter Co–Co distances of 2.62 and 2.63 Å (mean 2.67 Å). The fact that the six independent Co–S distances vary unrealistically from 2.05 to 2.20 Å provides crystallographic evidence for the existence of large systematic errors in this difficult structural determination.

(19) Wakatsuki, Y.; Okada, T.; Yamazaki, H.; Cheng, G. *Inorg. Chem.* **1988**, *27*, 2958–2963.

(20) (a) Rausch, M. D.; Genetti, R. A. *J. Org. Chem.* **1970**, *35*, 3888–3897. (b) Byers, L. R.; Dahl, L. F. *Inorg. Chem.* **1980**, *19*, 277–284.

(21) Bedard, R. L.; Dahl, L. F. *J. Am. Chem. Soc.* **1986**, *108*, 5933–5942.

(22) He, P.; Avery, J. P.; Faulkner, L. R. *Anal. Chem.* **1982**, *54*, 1313A–1326A.

(23) (a) Englert, M. H. Ph.D. Dissertation, University of Wisconsin—Madison, Madison, WI, 1984.

(24) Use of $CoCp(CO)_2$ in the reaction with CS_2 produced $Co_3Cp_3(\mu_3\text{-}S)_2$ (**2**) in similar yields.

(25) Madach, T.; Vahrenkamp, H. *Chem. Ber.* **1981**, *114*, 505–512.

(26) Reference for diamagnetic constants: *Landolt-Bornstein Tabellen, Neue Serie*, Bd II/2.

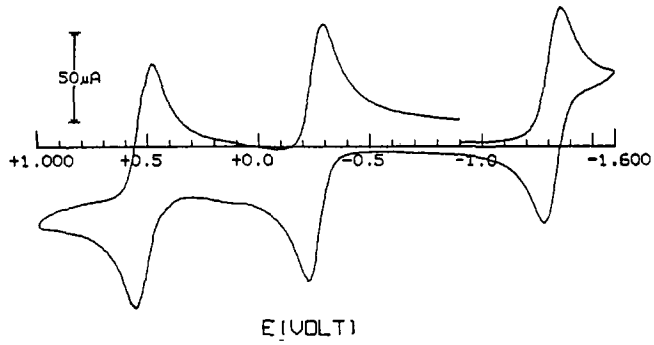

Figure 1. Cyclic voltammogram of $Co_3Cp'_3(\mu_3\text{-}S)_2$ (**1**) in CH_2Cl_2 at a scan rate of 200 mV/s. This current-voltage plot displays one reversible 1-electron reduction at $E_{1/2} = -1.31$ V ($\Delta E_p = 74$ mV) and two reversible 1-electron oxidations at $E_{1/2} = -0.26$ V ($\Delta E_p = 64$ mV) and $E_{1/2} = +0.52$ V ($\Delta E_p = 76$ mV). Voltages are measured relative to a saturated calomel electrode.

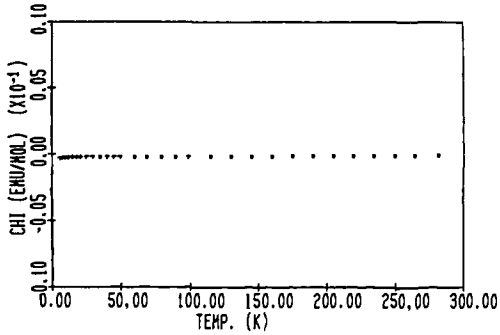

Figure 2. Plot of the molar magnetic susceptibility of $Co_3Cp'_3(\mu_3\text{-}S)_2$ (**1**) at 40 kG as a function of temperature from 6 to 280 K. This graph establishes that **1** is diamagnetic in the solid state and that the magnetic susceptibility is essentially temperature-independent.

(4) Solution Magnetic Susceptibility and Temperature-Dependent Proton NMR Data. Solution bulk magnetic susceptibility measurements of **1** were performed via the Evans method[27] in $CDCl_3$ on a Bruker WP 270-MHz NMR spectrometer. At 21 °C, an effective magnetic moment (corrected for metal and ligand diamagnetic susceptibilities[28]) of 1.05 μ_B was measured. The magnetic moment is 0.86 μ_B at 0 °C. A room-temperature ^1H NMR spectrum of **1** in 1:1 (v/v) CS_2/CD_2Cl_2 showed three broad singlets at δ 3.35 (3 H), 0.10 (2 H), and −1.45 (2 H). This occurrence of the proton resonances at different chemical shift values than those expected for a diamagnetic metal methylcyclopentadienyl complex, along with the increased signal widths, can readily be ascribed to the paramagnetic nature of **1** in solution. A ^1H NMR study of **1** from −105 to +35 °C showed large temperature dependences of the three proton resonances of the methylcyclopentadienyl rings (Figure 3). At the lowest temperature studied (−105 °C), normal diamagnetic methylcyclopentadienyl resonances were seen at δ 1.73 (3 H), 4.60 (2 H), and 4.70 (2 H). As the temperature of the sample was raised, the methyl resonance shifted downfield, while the two ring proton resonances moved upfield, until at +35 °C the resonances were δ 3.65 for the methyl protons and δ −0.87 and −2.80 for the two sets of ring protons.

$[Co_3Cp'_3(\mu_3\text{-}S)_2]^+[PF_6]^-$ ($1^+[PF_6]^-$). (a) Preparation. In a typical reaction, **1** (0.50 g, 1.05 mmol) and $AgPF_6$ (0.26 g, 1.03 mmol) were placed under N_2 in a flask containing a stir bar. Dichloromethane (20 mL) was added, and the solution was stirred at room temperature for 30 min. The solvent was then removed under vacuum and the dark gray residue extracted with hexane to remove any unoxidized **1**. Extraction with CH_2Cl_2, followed by filtration and solvent removal, gave the $[PF_6]^-$ salt of the monocation (1^+) in approximately 70% yield.

(b) Characterization and Properties. $1^+[PF_6]^-$ is soluble in most polar organic solvents such as CH_2Cl_2, THF, and CH_3CN. Cyclic voltammograms of this $[PF_6]^-$ salt of 1^+ in CH_2Cl_2 at 200 mV/s exhibited one reversible oxidation couple ($1+ \rightarrow 2+$, $E_{1/2} = 0.52$ V, $\Delta E_p = 83$ mV) and two reversible reduction couples ($1+ \rightarrow 0$, $E_{1/2} = -0.25$ V, $\Delta E_p = 75$ mV; $0 \rightarrow 1-$, $E_{1/2} = -1.33$ V, $\Delta E_p = 96$ mV). Solution bulk magnetic susceptibility measurements of $1^+[PF_6]^-$, determined via the Evans method[27] in $CDCl_3$, gave an effective magnetic moment (corrected for metal and ligand diamagnetic susceptibilities[28]) of 1.76 μ_B at 21 °C and 1.75 μ_B at −14.5 °C.

$[Co_3Cp'_3(\mu_3\text{-}S)_2]^{2+}[X]^-_2$, ($1^{2+}[X]^-_2$, X = PF_6, SbF_6). (a) Preparation. Since both the $[PF_6]^-$ and $[SbF_6]^-$ salts of 1^{2+} were analogously synthesized by oxidation of **1** with 2 equiv of the corresponding silver(I) salt, the following procedure is given only for obtaining $1^{2+}[PF_6]^-_2$. **1** (0.50 g, 1.05 mmol) in CH_2Cl_2 (20 mL) was added under N_2 into a flask containing $AgPF_6$ (0.53 g, 2.10 mmol). This mixture was stirred at room temperature for 45 min, during which time a dark gray precipitate formed. The solvent was then filtered off, and the residue was washed with CH_2Cl_2. Extraction of the remaining material with CH_3CN followed by filtration gave (after removal of the solvent) the $[PF_6]^-$ salt of the dication (1^{2+}) in approximately 60% yield.

(b) Characterization and Properties. The $[PF_6]^-$ and $[SbF_6]^-$ salts of 1^{2+} are soluble only in highly polar organic solvents such as acetonitrile and acetone. Cyclic and linear sweep voltammetric studies in CH_3CN confirmed that the salts contain the dication (1^{2+}). Three reversible reduction couples were expectedly observed for $1^{2+}[PF_6]^-_2$ in a cyclic voltammogram at 200 mV/s: viz., $2+ \rightarrow 1+$ at $E_{1/2} = 0.36$ V and $\Delta E_p = 52$ mV, $1+ \rightarrow 0$ at $E_{1/2} = -0.34$ V and $\Delta E_p = 67$ mV, and $0 \rightarrow 1-$ at $E_{1/2} = -1.32$ V and $\Delta E_p = 70$ mV. Two of the ΔE_p values are somewhat smaller than those seen in the cyclic voltammograms of **1** and the $[PF_6]^-$ salt of 1^+. This difference may be due to an overcompensation for solution resistance. Proton NMR measurements of $1^{2+}[SbF_6]^-_2$ in acetone-d_6 at room temperature displayed three normal singlet resonances of the methylcyclopentadienyl rings at δ 2.46 (3 H), 4.48 (2 H), and 4.69 (2 H). The closeness of the values for these methyl proton and two ring proton resonances to those for the corresponding limiting resonances observed at −105 °C for the diamagnetic isomer of **1** in solution is consistent with the expectation that the 48-electron 1^{2+} is also diamagnetic in solution. Initial attempts to grow crystals suitable for an X-ray diffraction study by the layering of diethyl ether onto a CH_3CN solution of the $[PF_6]^-$ salt of 1^{2+} gave crystals that were shown by cyclic and linear sweep voltammetry to contain 1^+ instead of 1^{2+}. Subsequently, crystals of $1^{2+}[SbF_6]^-_2$ were obtained for an X-ray crystallographic determination.

EPR Measurements of $Co_3Cp_3(\mu_3\text{-}S)_2$ (2), $Co_3Cp'_3(\mu_3\text{-}S)_2$ (1), and $[Co_3Cp'_3(\mu_3\text{-}S)_2]^+[PF_6]^-$ ($1^+[PF_6]^-$). All EPR spectra were recorded on a Varian E-15 spectrometer; diphenylpicrylhydrazyl (DPPH) was used as a reference for g value measurements. Solid **2**, prepared by the same method[24] used to make **1**, exhibited a broad, reasonably symmetric EPR resonance at room temperature with a line width of 2450 G, which narrowed to 1750 G at approximately 220 K. At ~160 K, the EPR resonance disappeared. Attempts to obtain EPR spectra of **1** and **2** in toluene solutions at room temperature and in frozen toluene solutions at −110 °C were unsuccessful.

A solution of $1^+[PF_6]^-$ in CH_2Cl_2 gave a single symmetric EPR signal at $g = 2.05$ (1) whose width of 220 G at room temperature narrowed to 116 G at approximately −20 °C. An EPR spectrum of a frozen CH_2Cl_2 solution at −110 °C was characteristic of an axially symmetric spin $^1/_2$ species with $g_\parallel = 2.16$ (1) and $g_\perp = 2.00$ (1).

X-ray Crystallographic Studies. (a) General Comments. Intensity data were collected for $Co_3Cp'_3(\mu_3\text{-}S)_2$ (**1**), $[Co_3Cp'_3(\mu_3\text{-}S)_2]^+[PF_6]^-$ ($1^+[PF_6]^-$), and $[Co_3Cp'_3(\mu_3\text{-}S)_2]^{2+}[SbF_6]^-_2$ ($1^{2+}[SbF_6]^-_2$) with either a refurbished Siemens (Nicolet) P$\bar{1}$ or a Siemens (Nicolet) P3F diffractometer with graphite-monochromated Mo Kα radiation ($\lambda = 0.7107$ Å). Details of crystal alignment and data collection are described elsewhere.[20b] Axial photographs were used to verify the approximate dimensions and symmetry of each unit cell. Scattering factors for neutral atoms were utilized with anomalous dispersion corrections for all nonhydrogen atoms. Crystal data collection and refinement parameters for each compound are given in Table I. Tables of positional parameters, anisotropic displacement coefficients, selected interatomic distances, and bond angles for the non-hydrogen atoms and idealized positional and fixed isotropic displacement coefficients for the hydrogen atoms are available for each compound as supplementary material along with a listing of observed and calculated structure factor amplitudes.

(b) $Co_3Cp'_3(\mu_3\text{-}S)_2$ (1). Black, single crystals of **1** were grown by slow evaporation of a benzene solution of the compound under N_2; a parallelepiped-shaped crystal (of dimensions 0.34 × 0.82 × 0.09 mm), epoxied inside an argon-filled Lindemann glass capillary, was used for data collection. Data were reduced[29] via a step-scan profile analysis and then were corrected for absorption by use of an analytical method.[30] The crystal structure was determined by application of direct methods in SHELXTL[31] followed by successive difference maps coupled with isotropic

(27) (a) Evans, D. F. *Proc. Chem. Soc.* **1958**, 115–116. (b) Evans, D. F. *J. Chem. Soc.* **1959**, 2003–2005. (c) Fritz, H. P.; Schwarzhans, K.-E. *J. Organomet. Chem.* **1964**, *1*, 208–211. (d) Live, D. H.; Chan, S. I. *Anal. Chem.* **1970**, *42*, 791–792. (e) Ostfeld, D.; Cohen, I. A. *J. Chem. Educ.* **1972**, *49*, 829. (f) Gerger, W.; Mayer, U.; Gutmann, V. *Monatsh. Chem.* **1977**, *108*, 417–422.

(28) Drago, R. S. *Physical Methods in Chemistry*; W. B. Saunders: Philadelphia, PA, 1977; p 413.

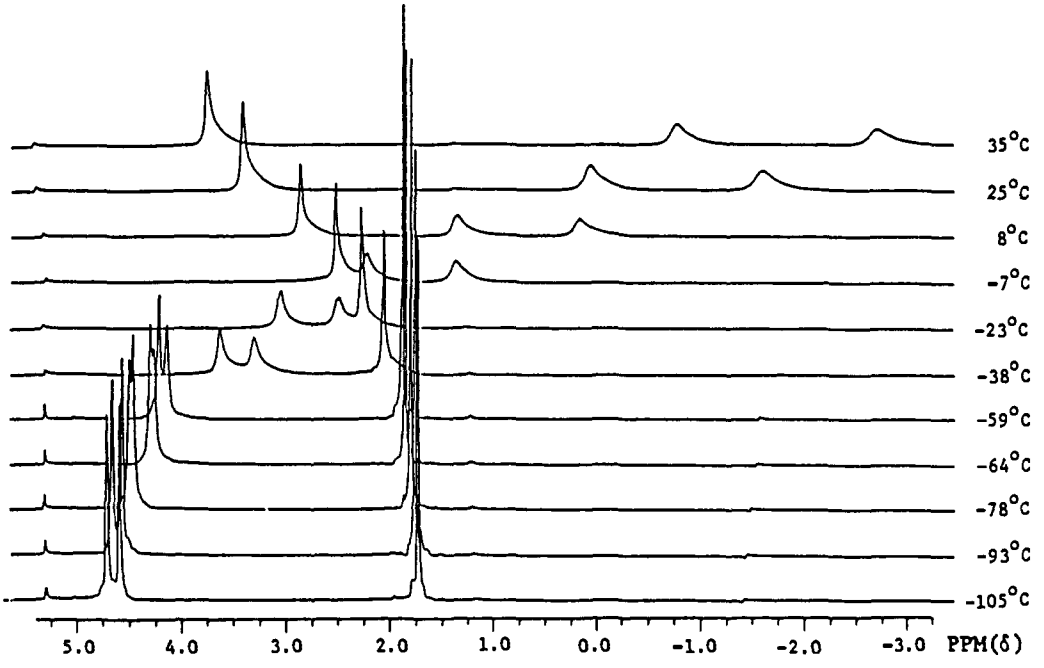

Figure 3. Variable-temperature 270-MHz ^1H NMR spectra of $Co_3Cp'_3(\mu_3\text{-}S)_2$ (**1**) in a 1:1 mixed CS_2/CD_2Cl_2 solution showing the dramatic temperature-dependent shifts of the Cp′ methyl proton and two Cp′ ring proton resonances from paramagnetic-induced values at 35 °C toward their diamagnetic-limiting values at −105 °C. With decreasing temperature the methyl proton signal shifts upfield from δ 3.65 (3 H) at 35 °C to 1.73 (3 H) at −105 °C, while the two ring proton signals shift downfield from δ −0.87 (2 H) and −2.80 (2 H) at 35 °C to δ 4.60 (2 H) and 4.70 (2 H), respectively, at −105 °C.

least-squares refinement. All non-hydrogen atoms were then refined anisotropically; hydrogen atoms with assigned isotropic temperature factors were included as fixed-atom contributors with calculated idealized positions based upon and moving with the positions of the attached carbon atoms. A final electron-density difference map did not reveal any unusual features.

(c) $[Co_3Cp'_3(\mu_3\text{-}S)_2]^+[PF_6]^-$ ($\mathbf{1}^+[PF_6]^-$). Black, single crystals of $\mathbf{1}^+[PF_6]^-$ were grown by a layering of hexane over a CH_2Cl_2 solution of the salt. X-ray data, obtained with a parallelepiped-shaped crystal of approximate dimensions 0.6 × 0.4 × 0.3 mm, were scaled for a 12% linear decay correction.[32] An absorption correction was made with ψ scans.[33] The crystal structure was determined by direct methods[34] followed by successive difference maps. Full-matrix least-squares refinement was performed with RAELS.[35] Each of the three methylcyclopentadienyl ligands was constrained such that the C–C distances within a particular ring were equal; however, the methyl carbon position was not constrained. Ring and methyl hydrogen atoms, calculated at idealized positions, were included with assigned isotropic temperature factors in the refinement as fixed-atom contributors. Both the positional parameters and the thermal motion of the three C_5H_4Me ligands were refined with subsidiary axial systems as described by Rae.[36] The thermal librational-like motion of each methylcyclopentadienyl ring was treated with a TLX group model.[37] All other non-hydrogen atoms were refined with individual anisotropic thermal parameters. A final difference map did not reveal any unusual features.

(d) $[Co_3Cp'_3(\mu_3\text{-}S)_2]^{2+}[SbF_6]^-_2$ ($\mathbf{1}^{2+}[SbF_6]^-_2$). Black crystals of $\mathbf{1}^{2+}[SbF_6]^-_2$ were grown by a layering of diisopropyl ether over an acetone

Table I. Crystallographic Data and Refinement Parameters for the 50/49/48-Electron $[Co_3Cp'_3(\mu_3\text{-}S)_2]^n$ Series (n = 0, 1+, 2+): $Co_3Cp'_3(\mu_3\text{-}S)_2$ (**1**), $[Co_3Cp'_3(\mu_3\text{-}S)_2]^+[PF_6]^-$ ($\mathbf{1}^+[PF_6]^-$), and $[Co_3Cp'_3(\mu_3\text{-}S)_2]^{2+}[SbF_6]^-_2$ ($\mathbf{1}^{2+}[SbF_6]^-_2$)

	1	$\mathbf{1}^+[PF_6]^-$	$\mathbf{1}^{2+}[SbF_6]^-_2$
formula weight	478.29	623.23	885.64
crystal system	orthorhombic	monoclinic	monoclinic
a, Å	31.050 (3)	18.577 (8)	6.886 (2)
b, Å	12.344 (2)	10.482 (3)	21.979 (6)
c, Å	19.119 (3)	22.735 (8)	17.892 (4)
β, deg	90.00	97.95 (3)	90.34 (2)
V, Å^3	7328 (2)	4380 (3)	2708 (1)
space group	*Pbca*	*C*2/*c*	$P2_1/c$
Z	16	8	4
d(calcd), g/cm^3	1.73	1.89	2.18
μ(Mo Kα), cm^{-1}	28.98	25.53	38.60
data collectn temp, °C	23	23	23
scan mode	θ–2θ	θ–2θ	Wyckoff ω
2θ limits, deg	3.0–50.0	3.0–55.0	3.0–50.0
scan speed, deg/min	variable; 4.0–29.0	variable; 3.0–29.0	variable; 3.0–29.0
background analysis	profile	profile	
no. check reflcts/freq	3/47	2/48	3/47
no. data collected	7193 (1 octant)	4234 (2 octants)	6202 (2 octants)
cutoff criterion	$I > 2.5\sigma(I)$	$I > 2.5\sigma(I)$	$F > 3.5\sigma(F)$
no. indep obs data	4398	3390	3610
no. parameters refined	415	247	307
$R_1(F)$, %; $R_2(F)$, %; GOF[a]	5.38; 9.42; 2.02	5.88; 7.19; 2.67	6.45; 7.18; 2.87

[a] $R_1(F) = [\sum||F_o| - |F_c||/\sum|F_o|] \times 100$; $R_2(F) = [\sum w_i||F_o| - |F_c||^2/\sum w_i|F_o|^2]^{1/2} \times 100$, where $w^{-1} = \sigma^2(F_o) + g(F_o)^2$; GOF = $[\sum w_i(|F_o| - |F_c|)^2/(m - n)]^{1/2}$, where m denotes the number of independent observed data and n denotes the number of refined parameters.

(29) Broach, R. W. CARESS, a Fortran Program for the Computer Analysis of Step-Scan Data. Ph.D. Thesis, University of Wisconsin—Madison, Madison, WI, 1977, Appendix I.

(30) (a) ALCOCK, N. W. Crystallographic Computing, Ottawa Summer School, 1969. (b) DeMeulenaer, J.; Tompa, H. *Acta Crystallogr.* **1965**, *19*, 1014–1018.

(31) (a) Sheldrick, G. M. In *Computing in Crystallography*; Schenk, H., Olthof-Hazekamp, R., Van Koningsveld, H., Bassi, G. C., Eds.; Delft University Press: Delft, 1978. (b) *Users Guide for SHELXTL*; Nicolet Analytical Instruments: Madison, WI, 1986.

(32) Broach, R. W. *QUICKSAM*, a FORTRAN Program for Sorting, Merging, and/or Decay Correction of Structure Factor Data. Ph.D. Thesis, University of Wisconsin—Madison, 1977, Appendix II.

(33) Christensen, A. FEEAR, a local subset of the data reduction routine TAPER, modified extensively for use at Wisconsin—Madison by R. W. Broach and C. Szmanda for the fast empirical evaluation for absorption regardless of crystal shape.

(34) Main, P.; Lessinger, L.; Woolfson, M. M.; Germain, G.; Declercq, J.-P. MULTAN-76, an updated version of MULTAN. Germain, G.; Main, P.; Woolfson, M. M. *Acta Crystallogr.* **1971**, *A27*, 368–376.

(35) Rae, A. D. RAELS, A Comprehensive Least-Squares Program, University of New South Wales, Kensington, 1976; Adapted for a Harris/7 Computer by A. D. Rae, University of Wisconsin—Madison, Madison, WI, 1984.

(36) Rae, A. D. *Acta Crystallogr.* **1975**, *A31*, 560–569.

(37) Rae, A. D. *Acta Crystallogr.* **1975**, *A31*, 570–574.

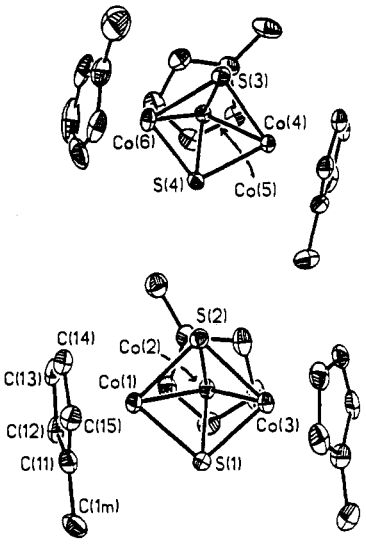

Figure 4. Molecular configurations of the two independent molecules of the 50-electron $Co_3Cp'_3(\mu_3\text{-}S)_2$ (**1**), which are distinguished from each other mainly by the different orientations of the methylcyclopentadienyl ligands. Each of their geometrically similar Co_3S_2 cores closely adheres to pseudo-C_{2v} symmetry with the isosceles cobalt triangle possessing one nonbonding edge of 3.19 Å (av) and two electron-pair bonding edges of 2.48 Å (av). All ring C(*np*) and methyl C(*nm*) labels (where n = 1–6; p = 1–5; m = CH_3) are analogous to those given for the ring attached to Co(1). Atomic thermal ellipsoids are drawn at the 30% probability level.

solution of the compound. A parallelepiped-shaped crystal of approximate dimensions 0.60 × 0.55 × 0.40 mm was used to obtain the X-ray data, to which an empirical absorption correction[33] based on 252 ψ scans was applied. The crystal structure was determined by direct methods[31] and subsequent difference maps. The ring carbon atoms of each Cp′ ring were constrained as a rigid group of D_{5h} symmetry with hydrogen atoms included in the least-squares refinements as fixed-atom contributors. A final difference map did not display any abnormal features.

Results and Discussion

Synthesis and Electrochemistry of $Co_3Cp'_3(\mu_3\text{-}S)_2$ (1). Both **1** and **2** were prepared in 15–20% yields by a convenient one-step synthesis that uses $Co(\eta^5\text{-}C_5H_{5-x}Me_x)(CO)_2$ (x = 0, 1) and the solvent CS_2 as the source of sulfur. This alternate synthetic route was discovered in connection with our research involving the metal-promoted head-to-head dimerization of carbon disulfide.[23,38] The original synthesis of **2** by Otsuka et al.[3] involved the reaction of $CoCp(CO)_2$ with $S(N^tBu)_2$ (where ^{t}Bu denotes t-C_4H_9) in refluxing heptane, from which $Co_3Cp_3(\mu_3\text{-}CO)(\mu_3\text{-}S)$, $Co_2Cp_2(\mu_2\text{-}(N^tBu)_2CO)$, and $(HN^tBu)_2CO$ were also obtained and separated from **2**.

Cyclic and linear sweep voltammetry revealed that the 50-electron **1** undergoes two chemically reversible oxidations to form the 49-electron monocation ($\mathbf{1}^+$) and 48-electron dication ($\mathbf{1}^{2+}$) and one chemically reversible reduction to form the 51-electron monoanion ($\mathbf{1}^-$). This electrochemical behavior is analogous to that observed for $Co_3Cp_3(\mu_3\text{-}S)_2$.[25] We prepared the hexafluorophosphate salts of both $\mathbf{1}^+$ and $\mathbf{1}^{2+}$ by the reaction of 1 and 2 equivs, respectively, of $AgPF_6$ with **1**. Since the members of the $[Co_3Cp'_3(\mu_3\text{-}S)_2]^n$ series (n = 2+, 1+, 0, 1−) possess no strong, identifying absorbances in the mid-infrared region that could be used to monitor the purity of the oxidation states of these compounds, linear sweep voltammetry (LSV) was utilized, in conjunction with cyclic voltammetry, to determine the purity of each compound. A mixture of these electroactive species will give residual current flow at all potentials in the linear sweep voltammogram, while a pure species will give an area without current flow in the potential range where that species is stable with respect to oxidation or reduction. Figure 1 displays a cyclic voltammogram of **1** in CH_2Cl_2. A linear sweep voltammogram of the pure neutral parent would show no residual current in the potential range from −0.4 to −1.2 V, a cathodic current at potentials more negative than −1.2 V, and an anodic current at potentials more positive then −0.4 V. Likewise, an LSV of the pure monocation ($\mathbf{1}^+$) would exhibit no residual current flow between +0.4 and −0.10 V, a current due to reduction at voltages more negative than −0.10 V, and a current due to oxidation at voltages more positive than +0.4 V. The null point for the pure dication ($\mathbf{1}^{2+}$) in CH_3CN occurs at voltages more positive than +0.5 V, while a cathodic current is observed at voltages more negative than +0.5 V.

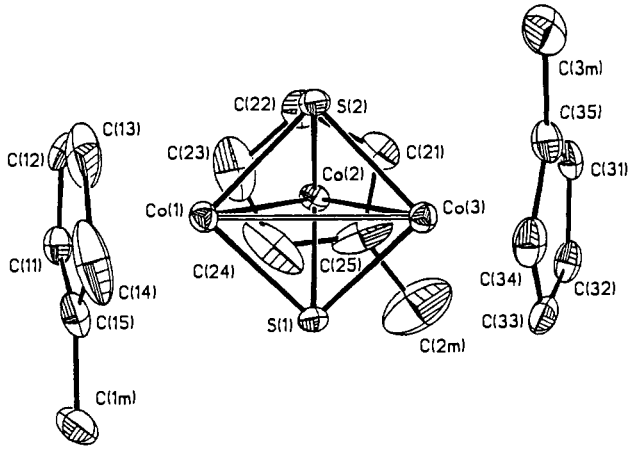

Figure 5. Configuration of the 49-electron $[Co_3Cp'_3(\mu_3\text{-}S)_2]^+$ monocation ($\mathbf{1}^+$) of the $[PF_6]^-$ salt. Its Co_3S_2 core ideally conforms to C_{2v} symmetry with the isosceles cobalt triangle possessing one "net 1-electron bonding" edge (denoted by a hollow line) of 2.87 Å and two electron-pair bonding edges of 2.49 Å (av). Atomic thermal ellipsoids are drawn at the 30% probability level.

Structural Features of $Co_3Cp'_3(\mu_3\text{-}S)_2$ (1). The unit cell of **1** contains two crystallographically independent molecules that are distinguished from each other mainly by the different orientations of one of the three methylcyclopentadienyl ligands (Figure 4). Each independent Co_3S_2 core closely conforms to C_{2v} symmetry with one nonbonding and two bonding Co–Co distances. Although the corresponding individual Co–Co distances of 2.492 (2), 2.497 (2), and 3.151 (2) Å for one molecule (A) are significantly different from those of 2.457 (2), 2.488 (2), and 3.221 (2) Å for the other molecule (B), the mean Co–Co distances of 2.713 and 2.722 Å for the two molecules are in good agreement. The two capping sulfur atoms in each molecule symmetrically bridge, within experimental error, the three cobalt atoms. The six Co–S distances in molecule A vary from 2.161 (3) to 2.179 (3) Å with a mean of 2.170 Å, while those in molecule B range from 2.166 (3) to 2.182 (3) Å with a mean of 2.179 Å. The average Co–C(ring) distance is 2.08 Å for each molecule with individual distances ranging from 2.03 (1) to 2.13 (1) Å.

Structural Features of $[Co_3Cp'_3(\mu_3\text{-}S)_2]^+[PF_6]^-$ ($\mathbf{1}^+[PF_6]^-$). This compound exists in the solid state as discrete cations and anions without any unusual interionic contacts. The crystallographically independent hexafluorophosphate anion possesses a normal octahedral configuration with the six P–F distances ranging from 1.487 (8) to 1.548 (6) Å (mean 1.53 Å). The cis F–P–F bond angles range from 85.6 (6) to 93.4 (5)° (mean 90.3°); the trans F–P–F bond angles vary from 177.4 (5) to 178.6 (6)° (mean 178.2°).

The Co_3S_2 core of $\mathbf{1}^+$ possesses an idealized C_{2v} geometry with no crystallographically imposed symmetry (Figure 5). The trimetal fragment can be readily described as an isosceles triangle with two shorter edges of 2.486 (1) and 2.495 (1) Å and one longer edge of 2.873 (1) Å. The mean of the three Co–Co distances is

(38) (a) $[Cp^*Ni]_2(\mu_2\text{-}C_2S_4)$: Maj, J. J.; Rae, A. D.; Dahl, L. F. *J. Am. Chem. Soc.* **1982**, *104*, 4278–4280. (b) $[Cp^*Co]_2(\mu_2\text{-}C_2S_4)$ and trans-$[Cp^*Fe(CO)]_2(\mu_2\text{-}C_2S_4)$: Englert, M. H.; Maj, J. J.; Rae, A. D.; Jordan, K. T.; Harris, H. A.; Dahl, L. F. *Abstracts of Papers*, 187th National Meeting of the American Chemical Society, St. Louis, MO; American Chemical Society: Washington, DC, 1984; INOR 280. (c) $[Cp_2Ti]_2(\mu_2\text{-}C_2S_4)$: Harris, H. A.; Rae, A. D.; Dahl, L. F. *J. Am. Chem. Soc.* **1987**, *109*, 4739–4741. Harris, H. A.; Kanis, D. R.; Dahl, L. F. *J. Am. Chem. Soc.*, in press.

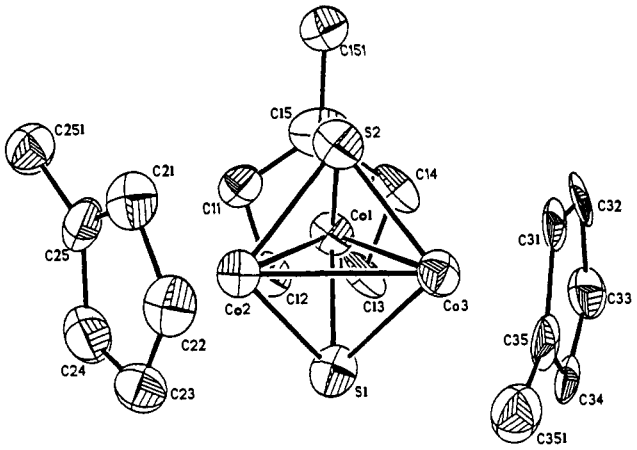

Figure 6. Configuration of the 48-electron $[Co_3Cp'_3(\mu_3\text{-}S)_2]^{2+}$ dication (1^{2+}) of the $[SbF_6]^-$ salt. Its Co_3S_2 core ideally conforms to D_{3h} symmetry with the pseudoequilateral cobalt triangle possessing three electron-pair bonding edges of 2.52 Å (av). Atomic thermal ellipsoids are drawn at the 30% probability level.

2.618 Å. The six experimentally equivalent distances from the cobalt atoms to the two triply bridging sulfur atoms range from 2.150 (2) to 2.161 (2) Å with a mean of 2.154 Å. The Co–C(ring) distances vary from 2.029 (5) to 2.113 (4) Å with an average value of 2.07 Å.

Structural Features of $[Co_3Cp'_3(\mu_3\text{-}S)_2]^{2+}[SbF_6]^-_2$ ($1^{2+}[SbF_6]^-_2$). The monoclinic unit cell of this compound contains four 1^{2+} dications and eight hexafluoroantimonate anions which pack under $P2_1/c$ symmetry with no abnormally short interionic contacts. Each of the two crystallographically independent $[SbF_6]^-$ anions expectedly has an octahedral configuration with the six Sb–F bond lengths ranging from 1.80 (3) to 1.86 (1) Å for one anion and from 1.82 (2) to 1.89 (2) Å for the other anion.

The configuration of the crystallographically independent 1^{2+} dication is displayed in Figure 6. Its Co_3S_2 core is considered to conform ideally to D_{3h} symmetry in spite of the small but significant variations in the three electron-pair bonding Co–Co distances of 2.485 (3), 2.533 (3), and 2.544 (3) Å (mean 2.521 Å). The two capping sulfur atoms are symmetrically coordinated to the three cobalt atoms; the six experimentally equivalent Co–S distances vary from 2.111 (5) to 2.127 (5) Å (mean 2.120 Å). The above determined distortion of the cobalt triangle from an equilateral geometry is *not* uncommon for a completely bonding 48-electron cluster with sterically innocent ligands; analogous variations in the three individual Co–Co distances from pseudo-3-fold symmetry have been found in other bicapped tricobalt clusters.[39] This observed deviation of only the cobalt triangle in the Co_3S_2 core from pseudo-D_{3h} symmetry may be a consequence of composite electronic–steric effects involving the noncylindrical Cp′ ligands.

A considerable variation is found in the 15 Co–C(ring) distances, which range from 2.00 (2) to 2.20 (1) Å (mean 2.08 Å). An examination of the individual Co–C(ring) distances for each of the three Cp′ ligands indicates that the extent to which a noncylindrical Cp′ ring is skewed from a symmetrical linkage to the attached cobalt atom is related to the relative orientation of its methyl substituent to the Co_3S_2 core. An unusually large asymmetry in the five Co–C(ring) distances (viz. from 2.00 (2) to 2.20 (1) Å) occurs for the Cp′ ligand coordinated to Co(1); as shown in Figure 6, its methyl group is directed nearly perpendicular to the tricobalt plane. In contrast, the Co–C(ring) distances for the Cp′ ligands attached to Co(2) and Co(3) exhibit much smaller ranges of 2.05 (1)–2.07 (1) and 2.04 (1)–2.11 (1) Å, respectively, in accordance with their methyl groups being situated much nearer to the tricobalt plane.

Proton NMR Study of $Co_3Cp'_3(\mu_3\text{-}S)_2$ (1) and Resulting Implications Concerning Its Magnetic Properties and Structure in Solution. (a) Experimental Evidence for Singlet–Triplet Spin Equilibrium. The temperature dependence of the three proton NMR resonances of the methylcyclopentadienyl ligands of **1** in a mixed CD_2Cl_2/CS_2 solution, shown in Figure 3, is consistent with a singlet–triplet spin equilibrium in solution. The room-temperature ^1H NMR spectrum showed three broad singlet resonances at δ 3.3 (3 H), 0.1 (2 H), and −1.5 (2 H). When the CD_2Cl_2/CS_2 solution of **1** was cooled to −105 °C, the methyl ^1H signal at δ 3.3 moved upfield to δ 1.7 and became a sharp singlet, while the ring ^1H signals at δ 0.1 and −1.5 sharpened while moving downfield to δ 4.6 and 4.7, respectively. There was no ^1H NMR evidence for a splitting of these resonances at lower temperatures into pairs of singlets with a 2:1 intensity ratio, which would be indicative of an instantaneous C_{2v} core geometry.

The temperature dependence of the paramagnetic shift of the NMR signals can be ascribed to the singlet–triplet spin equilibrium

$$\underset{\substack{\text{diamagnetic isomer}\\(S=0)}}{Co_3Cp'_3(\mu_3\text{-}S)_2\ \text{(singlet)}} \rightleftarrows \underset{\substack{\text{paramagnetic isomer}\\(S=1)}}{Co_3Cp'_3(\mu_3\text{-}S)_2\ \text{(triplet)}}$$

existing in solution, with the singlet-state isomer being the predominant form at, or below, room temperature. Experimental plots of the frequency shifts ($\Delta\nu$) as a function of temperature are presented in Figure 7 for the three proton resonances of **1**.

A similar temperature-dependent singlet–triplet spin equilibrium, which shifts to the singlet state at low temperature, was initially discovered[5,40] for the 50-electron **2** from variable-temperature ^1H NMR measurements and recently was reported by Wakatsuki et al.[19] for the 50-electron $Co_3(\eta^5\text{-}C_5H_4CO_2Me)_3(\mu_3\text{-}S)_2$. Of particular interest is that Wakatsuki et al.[19] also found from ^1H NMR solution measurements over a temperature range of +100 to −80 °C that the closely related 50-electron $Co_3(\eta^5\text{-}C_5H_4CO_2Me)_3(\mu_3\text{-}S)(\mu_3\text{-}N^tBu)$ (**3**) has a contrasting singlet–triplet equilibrium that shifts toward the triplet state at lower temperatures.[41] Singlet–triplet spin equilibria in solution have also been

(39) (a) $[Co_3(\eta^6\text{-}C_6H_6)_3(\mu_3\text{-}CO)_2]^+$ (Co–Co range 2.385 (4)–2.426 (4) Å): Olson, W. L.; Dahl, L. F. *J. Am. Chem. Soc.* **1986**, *108*, 7657–7663. (b) $[Co_3Cp'_3(\mu_3\text{-}NO)(\mu_3\text{-}NH)]^+[BPh_4]^-$ (Co–Co range 2.399 (3)–2.428 (3) Å): Bedard, R. L.; Dahl, L. F. *J. Am. Chem. Soc.* **1986**, *108*, 5942–5948. (c) $[Co_3Cp'_3(\mu_3\text{-}CO)(\mu_3\text{-}NC(O)NH_2]$ (Co–Co range 2.382 (1)–2.414 (1) Å): Bedard, R. L.; Rae, A. D.; Dahl, L. F. *J. Am. Chem. Soc.* **1986**, *108*, 5924–5932. (d) $Co_3Cp'_3(\mu_3\text{-}NO)_2$ (Co–Co range 2.395 (1)–2.414 (1) Å): Kubat-Martin, K. A.; Rae, A. D.; Dahl, L. F. *Organometallics* **1985**, *4*, 2221–2223.

(40) The cyclopentadienyl proton resonance observed for **2** in CS_2 solution from 163 to 324 K indicated diamagnetism below 173 K where the sharp singlet at δ 4.67 is virtually identical with that (δ 4.65) observed for the diamagnetic 48-electron $Co_3Cp_3(\mu_3\text{-}CO)(\mu_3\text{-}S)$ at ambient room temperature. With increasing temperature above 173 K, the signal was observed to broaden considerably upon undergoing a monotonic paramagnetic shift to higher field. A least-squares fit of the observed frequency shift/temperature data to a generalized form of the contact shift equation[5] was made.

(41) A solid-state magnetic susceptibility study[19] of $Co_3(\eta^5\text{-}C_5H_4CO_2Me)_3(\mu_3\text{-}S)(\mu_3\text{-}N^tBu)$ (**3**) from 18 to 294 K revealed that the molar susceptibility exhibits a broad maximum at 90 K; above this critical temperature the susceptibility was observed to approximately obey the Curie–Weiss law, while below this critical temperature the susceptibility curve falls rapidly with decreasing temperature to half the maximum value at 50 K. On the basis of the room-temperature X-ray diffraction analysis of **3**, which revealed a significant deformation of its metal framework from pseudo-C_{3v} symmetry (vide infra), Wakatsuki et al.[19] concluded that **3** has a singlet ground state at room temperature in the crystalline state. They proposed that the metal triangle of **3** is frozen in a distorted form by crystal packing forces but that in solution it could be relaxed to a configuration close to that of an equilateral metal triangle because its thermodynamically stable isomer in solution at low temperatures is the triplet isomer. Although Wakatsuki et al.[19] did not report effective magnetic moments based upon their susceptibility data, it is noteworthy that a calculated spin-only value of 2.74 μ_B is obtained from the molar susceptibility value at 300 K (taken from their solid-state magnetic susceptibility plot as a function of temperature). This μ_{eff} value signifies that, despite an indicated isosceles C_{2v} distortion from an idealized equilateral cobalt triangle, **3** has two unpaired electrons in the solid state at room temperature. We therefore suggest that solid **3** exists in the triplet state above the critical temperature (100 K) and in the singlet state below 100 K. This reinterpretation results in the solid-state magnetic susceptibility behavior of **3** being analogous to that of **2** (vide supra).[5] However, it is not compatible with the ^1H NMR paramagnetic shift data, which point to the triplet-state isomer being the thermodynamically stable isomer in solution at low temperatures (down to −80 °C). One possible explanation for this spin-state inversion in singlet–triplet behavior as a function of temperature is that the a_2' and e' levels (under assumed D_{3h} symmetry) are so close in energy that they interchange upon crystallization of **3** from solution due to anisotropic packing forces.

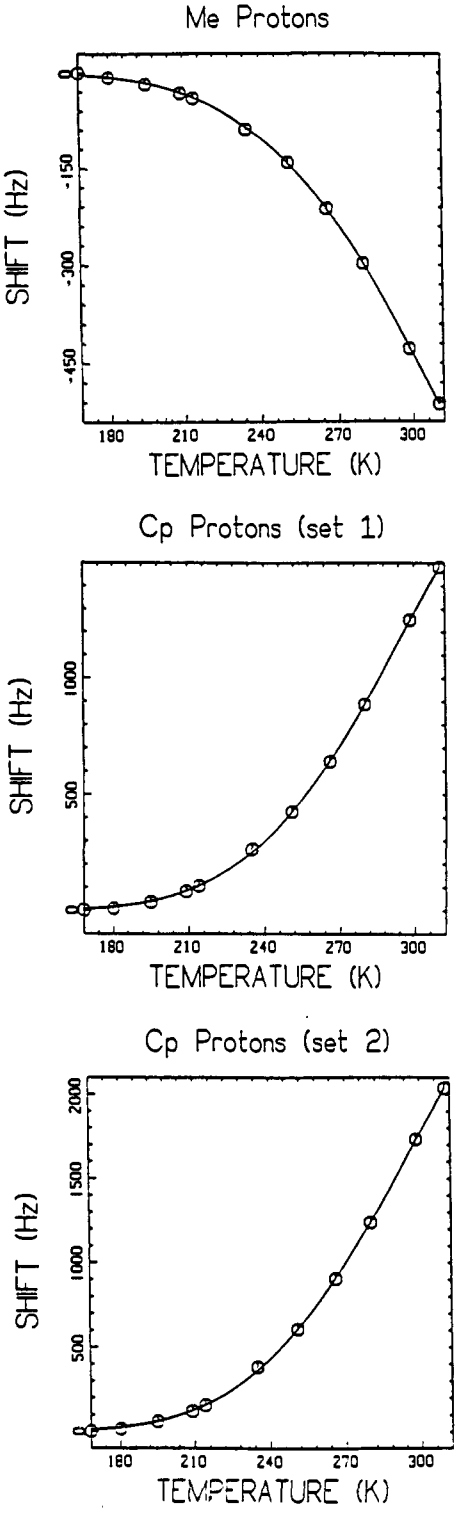

Figure 7. Temperature dependence of the isotropic shifts of the three methylcyclopentadienyl proton resonances in the 50-electron $Co_3Cp'_3$-$(\mu_3$-$S)_2$ (**1**): (top) frequency shift of the methyl proton signal as a function of temperature; (center) frequency shift of the ring proton signal (set 1) as a function of temperature; (bottom) frequency shift of the second ring proton signal (set 2) as a function of temperature. In each plot the solid line represents the least-squares fit of the data points to the general form of the contact shift equation, which was utilized to describe the singlet-triplet spin equilibrium of **1** in solution.

found for several 46-electron triangular metal clusters (i.e., the electron-deficient mirror images of the 50-electron triangular metal clusters). This paramagnetic shift behavior was initially demonstrated[11e] from a variable-temperature ^{1}H NMR study of $Co_3Cp^*_3(\mu_3$-$CO)_2$ ($Cp^* = \eta^5$-C_5Me_5). In contrast, $Co_3Cp_3(\mu_3$-$CO)_2$ was subsequently found by Barnes et al.[11d] to possess a single triplet spin state in solution over the entire temperature range studied (down to ca. 170 K); the fact that preliminary solid-state magnetic susceptibility measurements revealed that Co_3Cp_3-$(\mu_3$-$CO)_2$ becomes diamagnetic at temperatures below 100 K led Barnes et al.[11d] to conclude that the ground state may actually be a singlet.

Unanticipated thermal spin equilibria were recently reported[42] for two series of 46-electron heterometallic clusters of general formula $(MCp^*)_n(CoCp)_{3-n}(CO)_2$ (M = Co, Rh, Ir; n = 1, 2).[43] Of these six clusters, which were prepared and crystallographically–spectroscopically characterized in a comprehensive fashion by Barnes, Rheingold, Herrmann, and co-workers,[42] three were found in solution to possess temperature-dependent singlet–triplet spin equilibria displaced toward the singlet state at low temperatures. The other three clusters (M = Ir, n = 1; M = Ir, n = 2; M = Co, n = 2) exhibit linear increasing paramagnetic shifts with increasing inverse temperature; this Curie behavior is characteristic of only a triplet spin state in solution over the examined temperature ranges. However, Barnes et al.[42d] pointed out that it is unlikely that any of these three clusters is truly a ground-state triplet due to the consideration of their low symmetry (maximum C_{2v}) that excludes all but accidental orbital degeneracies. In addition, they stated that solid-state magnetic susceptibility measurements indicate that the ground state for the $IrCo_2$ cluster (n = 1) is a singlet and that the paramagnetic shifts observed for this cluster are derived from a spin equilibrium.[44]

(b) Theoretical Treatment of the Temperature-Dependent Isotropic Behavior and the Resulting Consequences. The analysis implemented herein to study the equilibrium between the two spin states of **1** is analogous to that described by Olson, Stacy, and Dahl[11e] for the singlet–triplet solution equilibrium for $Co_3Cp^*_3$-$(\mu_3$-$CO)_2$. It is also related to the earlier analyses utilized for a large number of d^8 nickel(II) bis(chelate) complexes by Phillips, Eaton, and co-workers[45] and by Holm and co-workers[46-49] to describe the solution configurational equilibrium between the diamagnetic, planar isomer with a singlet spin state and the paramagnetic, tetrahedral isomer with a triplet spin state. Each of these analyses involved the use of the contact shift equation[47-51]

(42) (a) Herrmann, W. A.; Barnes, C. E.; Zahn, T.; Zeigler, M. L. *Organometallics* **1985**, *4*, 172–180. (b) Horlein, R.; Herrmann, W. A.; Barnes, C. E.; Weber, C. *J. Organomet. Chem.* **1987**, *321*, 257–272. (c) Barnes, C. E.; Dial, M. R. *Organometallics* **1988**, *7*, 782–784. (d) Barnes, C. E.; Dial, M. R.; Orvis, J. A.; Staley, D. L.; Rheingold, A. L. *Organometallics* **1990**, *9*, 1021–1035.

(43) It is noteworthy that $(RhCp^*)_2(CoCp)(CO)_2$ is the only triangular metal cluster possessing approximately symmetrical triply bridging carbonyl ligands in the crystalline state; the two carbonyl ligands were viewed in each of the other five trimetal clusters as edge-bridging ligands that weakly interact with the third metal atom.[42d]

(44) The difficulty in establishing systematic trends in thermal spin behavior in solution is illustrated from the variable-temperature ^{1}H NMR paramagnetic shift data for the four 46-electron Cp^*/Cp tricobalt clusters, $Co_3Cp^*_{3-x}Cp_x(CO)_2$ (x = 0–3), which are formally related by the successive replacement of Cp^* with Cp ligands in $Co_3Cp^*_3(\mu_3$-$CO)_2$. Whereas the non-Cp-substituted (x = 0)[11e] and di-Cp-substituted (x = 2)[42d] tricobalt clusters possess a singlet–triplet solution equilibrium that shifts toward the singlet state at lower temperature, the mono-Cp-substituted (x = 1)[42d] and tri-Cp-substituted (x = 3)[11d] tricobalt clusters were found to have only a single triplet spin state in solution over the range studied. The fact that preliminary solid-state magnetic susceptibility measurements indicate that $Co_3Cp_3(\mu_3$-$CO)_2$ (x = 3) becomes diamagnetic at temperatures below 100 K led to the suggestion by Barnes et al.[11d] that its ground state is actually a singlet and that the observed paramagnetic shifts are derived from a singlet–triplet spin equilibrium.

(45) Eaton, D. R.; Phillips, W. D.; Caldwell, D. J. *J. Am. Chem. Soc.* **1963**, *85*, 397–406 and references cited therein.

(46) (a) Gerlach, D. H.; Holm, R. H. *J. Am. Chem. Soc.* **1969**, *91*, 3457–3467. (b) Powers, C. R.; Everett, G. W., Jr. *J. Am. Chem. Soc.* **1969**, *91*, 3468–3476. (c) Pignolet, L. H.; Horrocks, W. DeW., Jr.; Holm, R. H. *J. Am. Chem. Soc.* **1970**, *92*, 1855–1863 and references cited in these articles.

(47) Holm, R. H. *Acc. Chem. Res.* **1969**, *2*, 307–316 and references cited therein.

(48) Holm, R. H.; O'Connor, M. J. *Prog. Inorg. Chem.* **1971**, *14*, 241–401 and references cited therein.

(49) Holm, R. H.; Hawkins, C. J. In *NMR of Paramagnetic Molecules: Principles and Applications*; LaMar, G. N., Horrocks, W. DeW., Jr., Holm, R. H., Eds.; Academic Press: New York, 1973; pp 243–332.

to approximate the total isotropic shift for each unique proton nucleus.[52,53]

Unlike systems such as $Co_3Cp_3(\mu_3\text{-}S)_2$ (**2**) and $Co_3Cp^*_3(\mu_3\text{-}CO)_2$ where the ^1H NMR resonances reach a constant chemical shift at the lower temperatures studied, the shifts of the resonances in **1** did not appear, with any certainty, to come to a limiting, diamagnetic value. The value $\Delta\nu_i$ is defined as $\Delta\nu_i = \nu_s - \nu_{obsd}$, where ν_s is the proton resonance for the singlet-state, diamagnetic isomer and is taken to be the constant value of the resonance frequency reached at low temperature. If, at the lowest temperature studied, the measured ν_i is not the frequency of the pure singlet state, then $\Delta\nu_i$ will be off by a constant amount at all temperatures. Since this was clearly a possibility in the study of the equilibrium of **1**, a linear correction term (B_i) was included in the contact shift equation. Since A_i and g are constant for a given proton resonance of a system, the contact shift equation used in the nonlinear least-squares analysis was expressed as

$$\Delta\nu_i = (K_i'\nu_0/T)[\exp\{(\Delta H - T\Delta S)/RT\} + 1]^{-1} - B_i$$

where $K_i' = A_i(\gamma_e/\gamma_H)(g\beta S(S+1)/6Sk)$ is a constant for a given proton nucleus and B_i is the linear correction for the limiting diamagnetic resonance of the ith proton resonance. A positive value of B_i indicates that ν_s should be shifted B Hz downfield from its assumed position. This means that the new resonance frequency for the singlet, diamagnetic isomer is $\nu_s' = \nu_s + B$. The nonlinear least-squares fit of K_i', ΔH, ΔS, and B_i to the measured $\Delta\nu_i$ values at different temperatures resulted in the smooth curves through the data points displayed in the three plots in Figure 7. The converged least-squares parameters for each of the three proton signals are shown in Table II; a listing of observed and calculated shifts at different temperatures for the three proton resonances is available as supplementary material. The mean value of ΔH is 18.1 (3) kJ/mol, while ΔS has a mean value of 48 (4) J/mol·K. These values are very similar to ΔH = 18.1 (4) kJ/mol and ΔS = 50.2 (2) J/mol·K reported[11e] for the singlet–triplet solution equilibrium in $Co_3Cp^*_3(\mu_3\text{-}CO)_2$. The fact that ΔH is endothermic in each of these equilibria points to the thermodynamically stable isomer in solution at lower temperature being the singlet-state species. The large positive ΔS results in the triplet-state isomer existing in significant concentrations in solution at higher temperatures. Based upon the above mean values for the least-squares fitted ΔH and ΔS, the calculated mole fraction of the triplet spin state (N_t) of **1** in solution was found to vary dramatically over the temperature range investigated. The value of the mole fraction of the triplet state (N_t) is 0.0009 at 170 K, 0.05 at 250 K, 0.11 at 275 K, and 0.23 at the highest temperature investigated, 308 K. The value of ΔG also has a large temperature dependence. Based on the mean values found for ΔH and ΔS, the value of ΔG varies from 9.9 kJ/mol at 170 K to 3.3 kJ/mol at 308 K.

The assumption that the temperature-dependent isotropic shifts of **1** are principally contact in origin appears to be justified. The triplet states of the 50-electron **1** and **2** are each presumed to have D_{3h} Co_3S_2 core geometries in solution. The solid-state, room-temperature isomer of **2**, which has crystallographically imposed C_{3h} symmetry, has been shown to possess two unpaired electrons. A triplet-state isomer of D_{3h} symmetry requires an orbitally nondegenerate $^3A_2'$ ground state, for which dipolar shifts are usually considered to be negligible.[49,54] A spin-polarization mechanism, which arises from contact interactions, predicts that the direction of isotropic shifts reverses when a hydrogen atom is replaced by a methyl group.[49,54] This effect is seen in **1** where the methyl proton resonance moves upfield with decreasing temperature, while the two ring proton resonances move downfield. If the shifts were due to dipolar effects, which are geometrical effects, all the resonances would be expected to move in the same direction since their respective protons are in the same general area of the molecule. The directional shifts observed for **1** with decreasing temperature are in agreement with the downfield shifts with decreasing temperature found for the ring protons of **2** and the upfield shifts with decreasing temperature found[11e] for the methyl protons of the 46-electron $Co_3Cp^*_3(\mu_3\text{-}CO)_2$.[55]

Table II. Least-Squares Parameters for the Singlet–Triplet Equilibrium of $Co_3Cp'_3(\mu_3\text{-}S)_2$ (**1**) Obtained from Variable-Temperature ^1H NMR Spectra for Each Proton Signal Via the General Contact Shift Equation

^1H signal	$K_i'\nu_0$ (Hz·K)	ΔH (kJ/mol)	ΔS (J/mol·K)	B (Hz)
Me	−0.955 (2) × 10^6	17.90 (1)	44.41 (2)	−0.9 (5)
Cp(1)	1.689 (3) × 10^6	18.51 (1)	51.62 (2)	10 (1)
Cp(2)	2.374 (4) × 10^6	17.97 (1)	49.62 (2)	14 (2)
		18.1 (av)	48.6 (av)	

In order to make a comparison under identical treatments, the variable-temperature ^1H NMR data[5] of **2** were reanalyzed by use of the above generalized form of the contact shift equation. The proton NMR behavior of this compound in solution is almost identical with that exhibited by **1**. The nonlinear least-squares analysis of the variable-temperature ^1H NMR shift data for the one proton resonance of **2** (for which the linear correction term (B_i) was set equal to zero because the limiting diamagnetic proton signal was unambiguously observed) gave values of 16.99 (4) kJ/mol for ΔH and 50.7 (2) J/mol·K for ΔS. The closeness of these values to those determined for **1** conclusively establishes that **1** and **2** have analogous temperature-dependent paramagnetic shift behavior in solution even though their solid-state Co_3S_2 core geometries at room temperature are different. A listing of observed and calculated shifts at different temperatures for the proton resonance of **2** is available as supplementary material. Figure 8 displays the solid curve calculated for the observed proton shifts.

Solution Bulk Magnetic Susceptibility Studies of $Co_3Cp'_3(\mu_3\text{-}S)_2$ (1) and Its Monocation (1^+). A solution bulk magnetic susceptibility measurement of **1** in $CDCl_3$ at 21 °C gave an effective magnetic moment of 1.05 μ_B. This value, which is much smaller than the 2.83 μ_B expected for a molecule with two unpaired electrons, implies that at this temperature 14% of the molecules exist as the triplet isomer at any instant. These values compare well with a magnetic moment of 1.14 μ_B and a mole fraction (N_t) of 0.16, calculated by use of the mean of the three values for ΔH and for ΔS from the contact shift analysis and the relationship $N_t = (\mu_{eff}^2/\mu_t^2) = [\exp\{(\Delta H - T\Delta S)/RT\} + 1]^{-1}$, where μ_t, the magnetic moment for the triplet isomer, is assumed to have a spin-only value of 2.83 μ_B. At 0 °C, the solution susceptibility was 0.86 μ_B, which corresponds to N_t = 0.09. The resulting calculated values based on the mean ΔH and ΔS from the shift analysis are μ_{eff} = 0.89 μ_B and N_t = 0.10 at 0 °C. These results provide conclusive evidence that in solution the singlet-state (S

(50) Horrocks, W. DeW., Jr. *J. Am. Chem. Soc.* **1965**, *87*, 3779–3780.
(51) Eaton, D. R.; Phillips, W. D. *Adv. Magn. Reson.* **1965**, *1*, 103–149.
(52) For a paramagnetic isomer, the total isotropic shift, $(\Delta H_i/H_0)_{total}$ or $(\Delta\nu_i/\nu_0)_{total}$, of the ith proton nucleus is defined[47-51] as the sum of the contact and dipolar (pseudocontact) shifts: $(\Delta H_i/H_0)_{total} = (\Delta H_i/H_0)_{contact} + (\Delta H_i/H_0)_{dipolar}$; $(\Delta\nu_i/\nu_0)_{total} = (\Delta\nu_i/\nu_0)_{contact} + (\Delta\nu_i/\nu_0)_{dipolar}$. Our definition of the frequency shift of the ith nucleus is $\Delta\nu_i = \nu_s - \nu_{obsd}$, where ν_{obsd} is the observed frequency and ν_s the proton resonance for the singlet-state (diamagnetic) isomer. This definition is based on the convention[53] that a negative value of the paramagnetic shift $\Delta\nu_i$ represents a shift to lower applied magnetic field at a constant spectrometer frequency. Hence, for a constant magnetic field, $\Delta\nu_i = \nu_{dia} - \nu_{para}$, whereas ΔH_i is always defined as $\Delta H_i = \Delta H_{para} - \Delta H_{dia}$ for constant frequency.[53]
(53) Horrocks, W. DeW., Jr. In *NMR of Paramagnetic Molecules: Principles and Applications*; LaMar, G. N., Horrocks, W. DeW., Jr.; Holm, R. H., Eds.; Academic Press: New York, 1973; p 137.
(54) Horrocks, W. DeW., Jr. In *NMR of Paramagnetic Molecules: Principles and Applications*; LaMar, G. N., Horrocks, W. DeW., Jr., Holm, R. H., Eds.; Academic Press: New York, 1973; pp 127–177.
(55) Somewhat surprisingly, this variable-temperature ^1H NMR paramagnetic shift reversal effect when the five ring protons of a Cp ligand are replaced by five methyl substituents to form a Cp* ligand was not observed by Barnes et al.[42d] in their variable-temperature ^1H NMR studies of the 46-electron mixed Cp/Cp* $(MCp^*)_n(CoCp)_{3-n}(CO)_2$ clusters (M = Co, Rh, Ir; n = 1, 2). In the two tricobalt clusters (M = Co; n = 1, 2) as well as in the mixed-metal clusters, the signals for the Cp and Cp* protons were both shifted in the same direction as the temperature was changed. Barnes et al.[42d] suggested that contact π-delocalization mechanisms are not the only important contributions to the isotropic shift and that contact σ-delocalization mechanisms must also be considered.

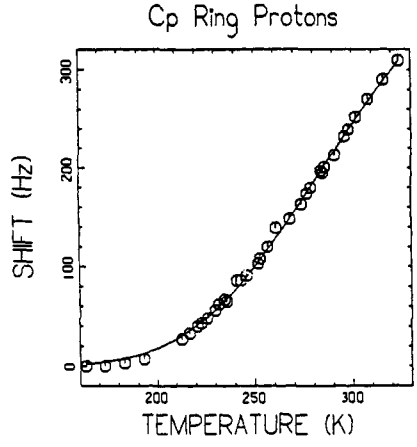

Figure 8. Plot of the isotropic frequency shift of the cyclopentadienyl proton resonance in the 50-electron $Co_3Cp_3(\mu_3\text{-}S)_2$ (**2**) as a function of temperature. The solid curve represents the least-squares fit of the data points, obtained by Frisch and Dahl,[5] to the general form of the contact shift equation presented herein. This reanalysis was carried out in order to compare the resulting thermodynamic parameters of **2** with those of **1** under identical treatments of the variable-temperature ^1H NMR data.

= 0) isomer predominates at low temperature but that as the temperature is raised, the concentration of the triplet-state isomer markedly increases.

A solution bulk magnetic susceptibility measurement of $\mathbf{1}^+[PF_6]^-$ in $CDCl_3$ exhibited an effective magnetic moment of 1.76 μ_B at 21 °C and 1.75 μ_B at −14.5 °C. The invariance of these values with temperature is expected for a species possessing one unpaired electron.

EPR Studies of $Co_3Cp_3(\mu_3\text{-}S)_2$ (2), $Co_3Cp'_3(\mu_3\text{-}S)_2$ (1), and $[Co_3Cp'_3(\mu_3\text{-}S)_2]^+[PF_6]^-$ ($\mathbf{1}^+[PF_6]^-$). For **2** as a solid, the observed broad EPR resonance that considerably narrows from room temperature to 220 K is in accordance with the solid-state magnetic susceptibility data, which have been interpreted in terms of a triplet electronic ground state for the molecule at these temperatures;[3-5] the disappearance of the EPR signal at low temperatures (e.g., at 160 K) is consistent with the observed phase transition of **2** to a diamagnetic structure below 192.5 K.[4] No EPR resonances were detected for solutions and frozen solutions of either **1** or **2**. Since the NMR data indicate that about 15% of each of these compounds in solution at room temperature should be in the triplet state, failure to observe solution EPR spectra is probably due to more rapid electron-spin relaxation and correspondingly broader lines in solution (as well as to a low concentration of the paramagnetic isomer).

The observance for $\mathbf{1}^+[PF_6]^-$ of a single symmetric EPR signal at $g = 2.05$ (1) in CH_2Cl_2 solution at room temperature and an anisotropic EPR spectrum with $g_\parallel = 2.16$ (1) and $g_\perp = 2.00$ (1) in frozen CH_2Cl_2 solution at −110 °C is consistent with the determined solid-state configuration of $\mathbf{1}^+$ being unaltered in solution. Detection of these EPR spectra necessitates that the one unpaired electron occupy a nondegenerate HOMO level sufficiently separated from the LUMO level such that a large broadening (and hence nondetection) of the EPR signal due to rapid electron-spin relaxation does not occur; a significant energy gap between the HOMO and LUMO is expected for the highly distorted C_{2v} Co_3S_2 core found in $\mathbf{1}^+[PF_6]^-$. The lack of resolved cobalt hyperfine structure in the EPR spectra of $\mathbf{1}^+[PF_6]^-$ precludes detailed conclusions concerning the number of equivalent cobalt atoms interacting with the unpaired electron and, hence, the specific cobalt orbital contributions to the HOMO. Of interest is that Enoki et al.[56] reported that the 49-electron $[Co_3Cp_3(\mu_3\text{-}CPh)_2]^-$ monoanion, generated by the reduction of the neutral 48-electron parent containing a Co_3C_2 core of pseudo-D_{3h} geometry,[57] exhibits a 22-line multiplet in both isotropic solution and anisotropic frozen-solution EPR spectra due to the hyperfine interaction of the unpaired electron with three equivalent cobalt nuclei ($I = {}^7/_2$, 100% abundance). The fact that the EPR spectra of the $[Co_3Cp_3(\mu_3\text{-}CPh)_2]^-$ monoanion displayed neither abnormal temperature dependence nor abnormal broadening led to the assignment of the unpaired electron to the in-plane trimetal-antibonding a_2' HOMO (under D_{3h} geometry); furthermore, its EPR parameters were found to compare favorably with those previously determined for the 49-electron $[Co_3(CO)_9(\mu_3\text{-}CPh)]^-$ anion[58] and 49-electron $Co_3(CO)_9(\mu_3\text{-}X)$ (X = S,[59] Se[60]); the unpaired electron in each of these two tricobalt carbonyl clusters was previously shown to reside in the analogous nondegenerate a_2 HOMO (under C_{3v} symmetry) which consists mainly of the antibonding combination of in-plane Co d_{xz} AOs.

Comparative Geometrical Analysis of Related Sulfur-Capped 50/49/48-Electron Triangular Cobalt Clusters and Resulting Bonding Implications. (a) General Remarks. The availability of geometrical data for all three members of the 50/49/48-electron $[Co_3Cp'_3(\mu_3\text{-}S)_2]^n$ series ($n = 0$, **1**; $n = 1+$, $\mathbf{1}^+$, $n = 2+$, $\mathbf{1}^{2+}$) provides for the first time highly convincing bond length evidence in support of our earlier hypothesis[5] that electrons in excess of the 48-electron count for a triangular metal cluster are trimetal-antibonding. A comparative analysis of Co–Co, Co–S, and Co–C(ring) distances presented in Table III for the structurally known members of the $[Co_3Cp'_3(\mu_3\text{-}S)_2]^n$ and $[Co_3Cp_3(\mu_3\text{-}S)_2]^n$ series and for related S-capped triangular cobalt clusters indicates an apparent correlation of Co–S and Co–C(ring) distances as well as Co–Co distances with the number of these "extra" antibonding valence electrons. It will be shown that current conclusions based upon previous MO analyses concerning the orbital nature and number of direct metal–metal interactions in such electron-rich triangular metal clusters are not in accordance with the observed electronic–geometrical changes in the $[Co_3Cp'_3(\mu_3\text{-}S)_2]^n$ series; a proposed solution interrelating the theoretical MO results with the localized valence-bond and electron-counting models for these metal clusters will be given.

(b) Structural-Bonding Comparison of the 50-Electron $Co_3Cp'_3(\mu_3\text{-}S)_2$ (1), $Co_3Cp_3(\mu_3\text{-}S)_2$ (2), and $Co_3(\eta^5\text{-}C_5H_4CO_2Me)_3(\mu_3\text{-}S)(\mu_3\text{-}N^tBu)$ (3). Each of the two crystallographically independent molecules A and B in **1** has a geometrically similar Co_3S_2 core, which closely conforms to C_{2v} symmetry; the resulting isosceles cobalt triangle for molecules A and B has one nonbonding edge of 3.15 and 3.22 Å, respectively, and two bonding edges of 2.49 (av) and 2.47 Å (av), respectively. This large separation of the two Co–Co distances in **1** clearly shows that the two electrons in excess of the electron count of 48 needed for a completely bonding trimetal core must occupy a trimetal-antibonding HOMO that is localized along the nonbonding Co···Co edge; furthermore, this nondegenerate MO must necessarily be antisymmetric with respect to the vertical mirror plane bisecting the long edge of the cobalt triangle in this 50-electron molecule. The two short Co–Co distances of 2.48 Å (av) for molecules A and B in **1** are similar to the one independent Co–Co distance of 2.45 Å in the 48-electron $Co_3Cp_3(\mu_3\text{-}S)(\mu_3\text{-}CO)$,[5] in accordance with the premise that these short Co–Co distances correspond to normal Co–Co single bonds.

The observed C_{2v} Co_3S_2 core geometry of each molecule in **1** can be rationalized in a bonding fashion similar to that presented by Rives et al.[13] for the structurally analogous C_{2v} Fe_3S_2 core in the diamagnetic 50-electron $Fe_3(CO)_9(\mu_3\text{-}S)_2$[15-17] with a $^1E(a_2'e')$ ground state (vide supra). Since the geometrical transformation

(56) $Co_3Cp_3(\mu_3\text{-}CPh)_2$: Enoki, S.; Kawamura, T.; Yonezawa, T. *Inorg. Chem.* **1983**, *22*, 3821–3824.

(57) The corresponding 48-electron $Co_3Cp_3(\mu_3\text{-}CR)(\mu_3\text{-}CR')$ (R = $SiMe_3$; R' = C≡$CSiMe_3$) of crystallographic C_1-1 site symmetry contains a Co_3C_2 core of pseudo D_{3h} symmetry: Fritch, J. R.; Vollhardt, K. P. C.; Thompson, M. R.; Day, V. W. *J. Am. Chem. Soc.* **1979**, *101*, 2768–2770.

(58) $[Co_3(CO)_9(\mu_3\text{-}CPh)]^-$: Peake, B. M.; Rieger, P. H.; Robinson, B. H.; Simpson, J. *Inorg. Chem.* **1979**, *18*, 1000–1005 and references therein.

(59) $Co_3(CO)_9(\mu_3\text{-}S)$: Wei, C. H.; Dahl, L. F. *Inorg. Chem.* **1967**, *6*, 1229–1236. (b) $Co_2Fe(CO)_9(\mu_3\text{-}S)$: Stevenson, D. L.; Wei, C. H.; Dahl, L. F. *J. Am. Chem. Soc.* **1971**, *93*, 6027–6031.

(60) $Co_3(CO)_9(\mu_3\text{-}X)$ (X = S, Se): (a) Strouse, C. E.; Dahl, L. F. *Discuss. Faraday Soc.* **1969**, *47*, 93–106. (b) Strouse, C. E.; Dahl, L. F. *J. Am. Chem. Soc.* **1971**, *93*, 6032–6041.

Table III. Structural Comparison at Room Temperature of Co_3S_2 Core Geometries for the 50/49/48-Electron $[Co_3Cp'_3(\mu_3\text{-}S)_2]^n$ Series (n = $[Co_3Cp(\mu_3\text{-}S)_2]^n$ **1**; n = 1+, **1**$^+$; n = 2+, **1**$^{2+}$) and 50/49-Electron $[Co_3Cp_3(\mu_3\text{-}S)_2]^n$ Series (n = 0, **2**; n = 1+, **2**$^+$) with Core Geometries for the 50-Electron $Co_3(\eta^5\text{-}C_5H_4CO_2Me)_3(\mu_3\text{-}S)(\mu_3\text{-}N^tBu)$ (**3**), 48-Electron $Co_3Cp_3(\mu_3\text{-}S)(\mu_3\text{-}CO)$ (**4**), 49-Electron $Co_3(CO)_9(\mu_3\text{-}S)$ (**5**), and 48-Electron $Co_2Fe(CO)_9(\mu_3\text{-}S)$ (**6**)

ref	compd	core valence electrons	M_3X_2 or M_3X core	crystallogr core symmetry	pseudo core symmetry	Co–Co distance (Å) individ	Co–Co distance (Å) mean	Co–S distance (Å) individ	Co–S distance (Å) mean	Co–C(ring) distance (Å) mean
a	**1**	50	Co_3S_2	C_1-1	C_{2v}	[2] 2.48 [1] 3.19	2.72	[4] 2.17 [2] 2.17	2.17	2.08
a	**1**$^+[PF_6]^-$	49	Co_3S_2	C_1-1	C_{2v}	[2] 2.49 [1] 2.87	2.62	[4] 2.15 [2] 2.15	2.15	2.07
a	**1**$^{2+}[SbF_6]^-_2$	48	Co_3S_2	C_1-1	D_{3h}	[3] 2.52	2.52	[6] 2.12	2.12	2.08
b	**2**	50	Co_3S_2	C_{3h}-3/*m*	D_{3h}	[3] 2.69	2.69	[6] 2.16	2.16	2.10
c	**2**$^+[I]^-$	49	Co_3S_2	C_s-*m*	C_{2v}	[2] 2.65 [1] 2.47	2.59	[4] 2.14 [2] 2.14	2.14	2.07
d	**2**$^+[SbF_6]^-$	49	Co_3S_2	C_{2v}-2*mm*	C_{2v}	[2] 2.64 [1] 2.52	2.60	[4] 2.15 [2] 2.14	2.15	2.06
e	**3**	50	Co_3SN	C_1-1	C_{2v}	[2] 2.60 [1] 2.54	2.58	[2] 2.16 [1] 2.15	2.16	2.11
c	**4**(disord)	48	Co_3SC	C_{3h}-3/*m*	D_{3h}[h]	[3] 2.45	2.45	[3] 2.27[i]	2.27[i]	2.07
f	**5**	49	Co_3S	C_1-1	C_{3v}	[3] 2.64	2.64	[3] 2.14	2.14	
g	**6**(disord)	48	Co_2FeS	C_1-1	C_{3v}	[3] 2.55	2.55	[3] 2.16[j]	2.16[j]	

[a] This work. [b] References 5 and 6. [c] Reference 5. [d] Reference 63. [e] Reference 19. [f] Reference 59a. [g] Reference 59b. [h] The labeled pseudo-D_{3h} core symmetry is a consequence of the crystal-disordered C_{3h} site symmetry being superimposed on the pseudo-C_{3v} core symmetry. [i] The unrealistically long independent Co–S bond length is due to a large systematic error arising from the crystallographically imposed C_{3h}-3/*m* site symmetry, which necessitates that the sulfur and carbonyl ligands are disordered into each other. [j] Small systematic errors in the Co–Co and Co–S distances arise for $Co_2Fe(CO)_9(\mu_3\text{-}S)$ (**6**) due to a presumed random 3-fold crystal disorder resulting in each labeled Co position actually being the composite of $^1/_3$Fe and $^2/_3$Co. The 0.02-Å longer mean Co–S distance than that in $Co_3(CO)_9(\mu_3\text{-}S)$ (**5**) is ascribed to the slightly larger covalent radius of Fe.

from D_{3h} to C_{2v} symmetry splits the doubly degenerate in-plane e′ MOs into two nondegenerate $a_1 + b_1$ MOs, the two antibonding electrons must occupy the $\sigma_v(yz)$-antisymmetric b_1 MO. The fact that solid-state magnetic susceptibility measurements showed that **1** is diamagnetic over the entire temperature range from 6 to 280 K is consistent with the energy level splitting being sufficiently large such that the two spin-paired antibonding electrons do not thermally populate the LUMO at higher temepratures. From a valence-bond viewpoint, the total metal–metal bond order (BO) of 2.0 for a 50-electron system is in agreement with **1** possessing one nonbonding Co···Co distance (corresponding to BO = 0) and two electron-pair Co–Co distances (corresponding to two individual BO = 1.0).

The average Co–Co distances of 2.71 and 2.72 Å for the two crystallographically independent molecules in **1** are similar to the independent Co–Co distance of 2.69 Å found in the 50-electron **2**, which in the crystalline state has an averaged structure of D_{3h} symmetry. A Co_3S_2 core possessing 3-fold symmetry would require that the two electrons in excess of the completely trimetal-bonding 48-electron configuration in **2** be delocalized over the three cobalt atoms giving rise to an equilateral cobalt triangle. From a valence-bond viewpoint, each of the three symmetry-equivalent Co–Co bonds would then possess a bond order of $^2/_3$. Molecular orbital calculations[13,19] indicate that under D_{3h} symmetry these two highest energy electrons in **2** would occupy two degenerate HOMOs corresponding to a triplet-state electronic configuration of either e'^2 or a composite $(a_2'e')^2$ at room temperature. Solid-state magnetic susceptibility studies[3-5] of **2** showed that the compound is paramagnetic at room temperature with two unpaired electrons. While it is possible that the observed equilateral cobalt triangle of **2** may be the result of a crystal disorder imposing C_{3h} site symmetry on a true C_{2v}-2*mm* or C_s-*m* molecular geometry, the sizes, shapes, and orientations of the thermal ellipsoids for the cobalt and sulfur atoms do not show any evidence of a crystal disorder.[5] While a disorder involving a small distortion of the Co_3S_2 core from a D_{3h} geometry would not be crystallographically detected, the observed averaged structure of **2** cannot be a 3-fold composite of the highly distorted isosceles cobalt triangle found in **1**; furthermore, such a structure would be diamagnetic instead of paramagnetic. Hence, we conclude that the triplet spin state isomer of **2** ideally possesses a D_{3h} Co_3S_2 core geometry.

The Co_3SN core of crystallographic C_1-1 site symmetry in the 50-electron $Co_3(\eta^5\text{-}C_5H_4CO_2Me)_3(\mu_3\text{-}S)(\mu_3\text{-}N^tBu)$ (**3**) was found[19] to possess a small but yet significant C_{2v}-type deformation from an idealized D_{3h} configuration, as indicated from one Co–Co bond length of 2.537 (1) Å being shorter than the other two Co–Co bond lengths of 2.587 (1) and 2.610 (1) Å.[41] That the mean Co–Co distance of 2.58 Å is markedly shorter than those in the electronically equivalent **1** (2.72 Å) and **2** (2.69 Å) is attributed mainly to a geometrical effect resulting from the formal substitution of a smaller capping NR ligand in place of one of the two capping S ligands.[61] A 0.07–0.09-Å shortening of the mean Co–Co distance likewise occurs when one of the two capping S atoms in the 48-electron **1**$^{2+}$ (2.52 Å) is formally replaced either by a smaller capping CO ligand (and two electrons) in the 48-electron $Co_3Cp_3(\mu_3\text{-}S)(\mu_3\text{-}CO)$ (2.45 Å)[5] or by a similarly smaller capping CS ligand (and two electrons) in the 48-electron $Co_3Cp_3(\mu_3\text{-}S)(\mu_3\text{-}CS)$ (2.43 and 2.44 Å for two independent molecules).[62]

(c) Structural-Bonding Comparison of the 49-Electron $[Co_3Cp'_3(\mu_3\text{-}S)_2]^+[PF_6]^-$ (1$^+[PF_6]^-$) and $[Co_3Cp_3(\mu_3\text{-}S)_2]^+[X]^-$ (2$^+[X]^-$; X = I, SbF_6). These **1**$^+$ and **2**$^+$ monocations contain 49 valence cluster electrons, one more than is in a completely trimetal-bonding Co_3S_2 cluster. The **1**$^+$ monocation in the $[PF_6]^-$ salt possesses two normal Co–Co electron-pair bonding distances of 2.49 and 2.50 Å and one longer distance of 2.87 Å. This latter value, which is midway between the lengths of the nonbonding and normal bonding edges in the neutral parent (**1**), implies a local valence metal–metal bond order of 0.5 and a total metal–metal bond order of 2.5 in agreement with a 49-electron triangular metal system having one antibonding and six bonding electrons.

On the other hand, the **2**$^+$ monocations in both the $[I]^-$ salt[5] and $[SbF_6]^-$ salt,[63] which have crystal-required C_s-*m* and C_{2v}-2*mm* site symmetry, respectively, possess one normal Co–Co electron-pair bonding distance and two longer Co–Co distances. The

(61) It is noteworthy that the shorter mean Co–Co distance in $Co_3(\eta^5\text{-}C_5H_4CO_2Me)_3(\mu_3\text{-}S)(\mu_3\text{-}N^tBu)$ (**3**) may also be partially due to the electron-withdrawing CO_2Me substituent of each $C_5H_4CO_2Me$ ring, which should decrease the tricobalt-antibonding electron density in the tricobalt framework through greater charge delocalization onto the $C_5H_4CO_2Me$ ligands. An operational test of the importance of this electronic effect would be to carry out an X-ray crystallographic determination of $Co_3(\eta^5\text{-}C_5H_4CO_2Me)_3(\mu_3\text{-}S)_2$, which was prepared by Wakatsuki et al.[19] for variable-temperature ^{1}H NMR solution measurements.

(62) $Co_3Cp_3(\mu_3\text{-}S)(\mu_3\text{-}CS)$: Werner, H.; Leonhard, K.; Kolb, O.; Röttinger, E.; Vahrenkamp, H. *Chem. Ber.* **1980**, *113*, 1654–1662.

(63) $[Co_3Cp_3(\mu_3\text{-}S)_2]^+[SbF_6]^-$: Teo, B.-K. Ph.D. dissertation, University of Wisconsin—Madison, Madison, WI, 1973.

two virtually identical longer distances of 2.65 Å in the $[I]^-$ salt and 2.64 Å in the $[SbF_6]^-$ salt are 0.22 Å shorter than the single long Co–Co distance of 2.87 Å in $1^+[PF_6]^-$, for which BO = 0.5. Each of these two longer Co–Co distances in the $[I]^-$ and $[SbF_6]^-$ salts of 2^+ is completely consistent with a local valence metal–metal bond order of $^3/_4$; the resulting total metal–metal bond order of 2.5 is the same as that experimentally deduced for 1^+.

A salient geometrical feature is that the isosceles cobalt triangle in 1^+ with one longer and two shorter electron-pair bonds is the inverse of that in 2^+ with one shorter electron-pair bond and two longer bonds. On the basis of these inverted isosceles cobalt triangles, it follows that the nature of the HOMO containing the unpaired electron must be different in 1^+ and 2^+. In the case of 1^+ the 49th electron must occupy a HOMO (of b_1 representation under C_{2v} symmetry) which is *antisymmetric* with respect to the vertical $\sigma_v(yz)$ mirror plane, whereas in 2^+ the 49th electron is in a HOMO (of a_1 representation under C_{2v} symmetry), which is *symmetric* with respect to the vertical $\sigma_v(yz)$ mirror plane bisecting the isosceles cobalt triangle.

Of interest is that the 49-electron $Co_3Cp'_3(\mu_3\text{-}NO)(\mu_3\text{-}NH)$[64] of pseudo-$C_s$ symmetry has a C_{2v} isosceles cobalt triangle with one longer and two normal shorter Co–Co bonds like that seen for the $[Co_3Cp'_3(\mu_3\text{-}S)_2]^+$ monocation (1^+). These results establish that the electronic differences between the cylindrical Cp ligand and the noncylindrical Cp′ ligand can play a decisive role in dictating the type of isosceles metal triangle formed for the 49- and 50-electron systems. In contrast to the cylindrical Cp ligands, the noncylindrical Cp′ ligands presumably split the degeneracy of the frontier e′ MOs of the Co_3S_2 core such that under C_{2v} symmetry the trimetal-antibonding electron occupies the lower energy b_1 level in the 49-electron 1^+.

The fact that the mean Co–Co bond distances in the 49-electron monocations of $1^+[PF_6]^-$ (2.62 Å), $2^+[SbF_6]^-$ (2.60 Å), and $2^+[I]^-$ (2.59 Å) are close to one another shows that the total metal–metal bonding character in the two inverted isosceles cobalt triangles is consistent within these corresponding members of the two series even though the individual Co–Co distances are quite different. The corresponding mean Co–S and Co–C(ring) distances in the monocations for the three salts are also in good agreement with one another. The mean Co–S distances in the monocations of $1^+[PF_6]^-$, $2^+[SbF_6]^-$, and $2^+[I]^-$ are 2.15, 2.14, and 2.15 Å, respectively, while the mean Co–C(ring) distances in the monocations of $1^+[PF_6]^-$, $2^+[SbF_6]^-$, and $2^+[I]^-$ are 2.07, 2.07, and 2.06 Å, respectively.

(d) Structural-Bonding Analysis of 50/49/48-Electron $[Co_3Cp'_3(\mu_3\text{-}S)_2]^n$ Series and 50/49-Electron $[Co_3Cp_3(\mu_3\text{-}S)_2]^n$ Series and Resulting Implications Regarding Molecular Orbital Interpretations. That the 49th and 50th valence cluster electrons in both the $[Co_3Cp'_3(\mu_3\text{-}S)_2]^n$ and $[Co_3Cp_3(\mu_3\text{-}S)_2]^n$ series are trimetal-antibonding is unequivocally established for the first series from the fact that oxidations of **1** to 1^+ and 1^+ to 1^{2+} decrease the mean Co–Co distance by 0.10 Å in each case. Similarly, an oxidation of **2** to 2^+ also decreases the mean Co–Co distance by 0.10 Å.

An examination of Table III reveals that the 1-electron oxidations of **1** to 1^+ and 1^+ to 1^{2+} also result in successive concomitant bond length decreases of 0.02 and 0.03 Å, respectively, in the mean value of the much stronger Co–S bonds. This small but yet highly significant bond length trend, which is likewise observed upon oxidation of **2** to 2^+, supports the premise that the e′ MOs in **1** and **2** (under assumed D_{3h} symmetry) have significant antibonding Co–S orbital character. Table III also indicates an analogous pattern of 0.01–0.02-Å decreases in the mean Co–C(ring) distances upon successively going from 50- to 49- to 48-electron tricobalt clusters. The resulting prediction that the frontier a_2' and e′ MOs would also have significant Co–C(ring) antibonding orbital character is in accordance with MO calculations.

While these experimentally deduced bonding conclusions substantiate the validity of the electron-counting and valence-bond models, which intrinsically assume that these extra electrons are trimetal-antibonding, they are incompatible with the current conclusion[13] resulting from the Fenske–Hall MO calculations that the orbital nature of direct metal–metal interactions in the frontier e′ MOs of **2** (under assumed D_{3h} symmetry) is trimetal-bonding instead of trimetal-antibonding. This conclusion is based upon the major orbital contributions to these frontier e′ MOs being the trimetal-bonding in-plane Co d_{xz} AOs.[65] In order to make the MO calculations congruent with the experimentally deduced valence-bond analysis, it is necessary to assume that the minor trimetal-antibonding contributions of the Co 4s and $4p_z$ AOs to the e′ MOs dominate in causing the observed redox-generated changes in geometry in these electron-rich triangular metal clusters.[65-68]

Conclusions

A new method for the preparation of **1** and **2** is given. This synthetic route allows for an easier separation of the desired compound from the other reaction products than did the previous method utilized[3-5] to obtain **2**.

The solid-state structure of the 50-electron $Co_3Cp'_3(\mu_3\text{-}S)_2$ (**1**) possesses an idealized C_{2v} molecular geometry consisting of an isosceles cobalt triangle with one nonbonding edge of 3.19 Å and two electron-pair bonding edges of 2.48 Å. Hence, the two extra trimetal-antibonding electrons must be localized along the nonbonding Co–Co edge in a nondegenerate MO that is antisymmetric with respect to the mirror plane passing through the third cobalt atom and the two capping sulfur atoms. This molecular geometry is in accordance with the solid-state magnetic susceptibility measurements between 6 and 280 K, which unambiguously show that **1** is diamagnetic over the entire temperature range. If the observed increase in the solution paramagnetism of **1** with increasing temperature were, in fact, due to thermal population of a triplet excited state, then the solid-state magnetic moment would also be expected to increase with increasing temperature. The temperature-independent diamagnetism of **1** in the solid state provides convincing evidence that its solution magnetic properties

(64) $Co_3Cp'_3(\mu_3\text{-}NO)(\mu_3\text{-}NH)$: Bedard, R. L.; Dahl, L. F. *J. Am. Chem. Soc.* **1986**, *108*, 5942–5948.

(65) The orbital designations utilized in the MO calculations[13] of **2** are based upon localized right-handed coordinated axes at each cobalt atom being chosen with the *z*-axis pointing to the centroid of the cobalt triangle and with the *x*-axis lying in and the *y*-axis perpendicular to the tricobalt plane. Of the Co valence AOs transformed under D_{3h} symmetry into symmetry-adapted combinations, the orbital character of the frontier a_2' and e′ MOs may consist of the following cobalt valence AOs: a_2' ($3d_{xy}$, $4p_y$); e′ ($3d_{z^2}$, $3d_{x^2-y^2}$, $3d_{xy}$, 4s, $4p_x$, $4p_y$). Of the Co valence orbitals that belong to the e′ representation, the $3d_{z^2}$, $3d_{x^2-y^2}$, 4s, and $4p_z$ combinations are trimetal-antibonding while the $3d_{xz}$ and $4p_x$ combinations are trimetal-bonding. For the a_2' representation, both the Co $3d_{xz}$ and $4p_x$ combinations are trimetal-antibonding.

(66) It is noteworthy that Rives et al.[13] also employed the natural hybrid orbital (NHO) technique developed by Weinhold and co-workers[67] to analyze their MO results from the Fenske–Hall method. Their initial NHO calculations, in which the metal atoms were treated individually, failed not only in describing direct localized M–M bonding but also in describing the direct metal atom to bridging ligand bonding. Consequently, they performed a second NHO analysis[13] in which the three metal atoms are grouped together as one substrate unit (M_3); of significance is that the metal contributions in both the M_3–μ_3-S σ and π bonds, which involve delocalized acceptor hybrids on the tricobalt fragment accepting electron density from donor orbitals on the capping sulfide atoms, were found to be composed primarily of 4s and 4p metal AOs. For **2** the percent characters of the trimetal-delocalized hybrids were 24% 3d, 22% 4s, and 54% 4p in the $\sigma_{Co_3\text{-}S}$ bonds and 43% 3d, 12% 4s, and 45% 4p in the $\pi_{Co_3\text{-}S}$ bonds. Rives et al.[13] suggested that the metal valence 4s and 4p AOs dominate the metal–metal interactions in the Co_3S_2 core; they also pointed out that the delocalized-hybrid description of the metal acceptor orbitals is *not unrelated* to the Lauher cluster valence MO (CVMO) model,[68] which involves CVMOs of predominantly s and p AO character. These theoretically based conclusions are in harmony with our conclusive experimental evidence that the observed structural changes in the 50- and 49-electron Co_3S_2 clusters are controlled by the more diffuse and better overlapping trimetal-antibonding combinations of cobalt 4s and 4p AOs. Unfortunately, Rives et al.[13] wrongly concluded from their Fenske–Hall calculations that the e′ HOMOs for these clusters are trimetal-bonding due to the $3d_{xz}$ AO combinations being the major contributors.

(67) (a) Foster, J. P.; Weinhold, F. *J. Am. Chem. Soc.* **1980**, *102*, 7211–7218. (b) Rives, A. B.; Weinhold, F. *Int. J. Chem. Symp.* **1980**, *14*, 201–209; *Ibid.* **1981**, *15*, 555. (c) Reed, A. E.; Weinstock, R. B.; Weinhold, F. *J. Chem. Phys.* **1985**, *83*, 735–746. (d) Reed, A. E.; Curtiss, L. A.; Weinhold, F. *Chem. Rev.* **1988**, *88*, 899–926.

(68) Lauher, J. W. *J. Am. Chem. Soc.* **1978**, *100*, 5305–5315.

are due not to thermal population of a triplet state but to a temperature-dependent spin equilibrium between a diamagnetic isomer and a paramagnetic isomer.

In contrast, the corresponding 50-electron **2** exhibits a solid-state magnetic susceptibility of 2.8 μ_B at room temperatures corresponding to two unpaired electrons. This paramagnetism is completely consistent with the Co_3S_2 core in this molecular complex of crystallographic C_{3h}-3/*m* site symmetry ideally possessing a D_{3h} geometry with an equilateral cobalt triangle (which may be slightly deformed toward an isosceles cobalt triangle, as found in **3**, due to a *small* instantaneous C_{2v} molecular distortion).

That the variable-temperature solution ^{1}H NMR behavior of **1** is nearly identical with that of **2** further supports the contention that in solution a diamagnetic isomer of idealized C_{2v} geometry is in equilibrium with a paramagnetic isomer of presumed idealized D_{3h} geometry. The large similar ΔS values in **1** and **2** calculated from the least-squares analysis of the ^{1}H NMR shift data, which make ΔG strongly temperature-dependent, also suggest a marked geometrical change between the singlet- and triplet-state isomers in both **1** and **2**. The observations that **2** has two unpaired electrons at room temperature in the crystalline state but yet in solution exhibits a singlet–triplet spin equilibrium with the majority of molecules being in the singlet state at room temperature are difficult to reconcile. Since **2** becomes diamagnetic at low temperatures in both solution and solid state, its ground state must be a singlet, as is also observed for **1**. The existence of both isomers of **2** in solution at room temperature in contrast to only the paramagnetic isomer in the solid at that temperature is presumed to reflect a small difference between the energies of the singlet and triplet states. On the other hand, the magnetic–structural properties of **1** in solution are consistent with those in the solid state.

Oxidations of **1** to its monocation ($\mathbf{1}^+$) and dication ($\mathbf{1}^{2+}$) result in the successive removal of both trimetal-antibonding electrons from the HOMO, as evidenced by X-ray crystallographic determinations of the isolated $\mathbf{1}^+[PF_6]^-$ and $\mathbf{1}^{2+}[SbF_6]^-_2$ compounds; large decreases in the long Co–Co distance by 0.32 Å from **1** (3.19 Å) to $\mathbf{1}^+$ (2.87 Å) and by 0.35 Å from $\mathbf{1}^+$ to $\mathbf{1}^{2+}$ (2.52 Å) are found along with only slight concomitant increases of 0.01 and 0.03 Å, respectively, in the two short electron-pair Co–Co distances. These 1-electron oxidations of the 50-electron **1** to $\mathbf{1}^+$ and then to $\mathbf{1}^{2+}$ also give rise to successive concomitant bond length decreases of 0.02 and 0.03 Å, respectively, in the mean value of the Co–S bonds (Table III). These small but yet highly significant changes in the much stronger Co–S bonds support the premise that the HOMO in the neutral parent (**1**) likewise has significant antibonding Co–S orbital character. From a valence-bond viewpoint, these redox-generated changes in geometry correspond to an increase in the metal–metal bond order of the long Co–Co edge from 0.0 for **1**, to 0.5 for $\mathbf{1}^+$, and to 1.0 for $\mathbf{1}^{2+}$ with no change in the metal–metal bond order of 1.0 for each of the other two equivalent Co–Co edges (under assumed C_{2v} symmetry).

A correlation of the *mean* Co–Co distances in the 50-electron **1**, **2**, and **3** with those in the 49-electron $\mathbf{1}^+$ and $\mathbf{2}^+$ and in the 48-electron $\mathbf{1}^{2+}$ and the other related S-capped tricobalt clusters provides convincing evidence for the validity of the electron-counting and valence-bond models, which are based upon the inherent assumption that the HOMOs for the 49- and 50-electron triangular metal systems invariably have trimetal-antibonding orbital character. The indicated incompatibility of these structural-bonding analyses with previous theoretical MO interpretations of **2**, $\mathbf{2}^+$, and related S-capped triangular metal clusters is scrutinized. The previous conclusion[13] resulting from the Fenske–Hall MO calculations that the orbital nature of direct metal–metal interactions in the frontier e′ MOs of **2** and $\mathbf{2}^+$ (under assumed D_{3h} symmetry) is trimetal-bonding (instead of trimetal antibonding) is based entirely upon the major contributions to these frontier e′ MOs being the trimetal-bonding in-plane Co d_{xz} AOs. In order to resolve this important problem in relating "theoretical quantum mechanics" with "experimental quantum mechanics", it is necessary to assume that the minor trimetal-antibonding contributions of the Co 4s and Co $4p_z$ AOs to the e′ MOs dominate in causing the observed structural changes generated by the reversible electron-transfer processes in these electron-rich metal clusters. This commanding influence of the more diffuse Co 4s and 4p valence AOs over the contracted Co 3d AOs is readily attributed to much better orbital overlap at long metal–metal distances.[66-68]

Acknowledgment. This research was supported by the National Science Foundation (Grants CHE-8616697 and CHE-9013059). We are grateful to Professor A. David Rae (School of Chemistry, University of New South Wales, Kensington, Australia) for his aid in the use of his least-squares program RAELS. We are also indebted to Dr. Bruce R. Adams and Mr. John M. Bemis (UW—Madison) for their assistance in the proton NMR measurements and to Dr. Kenneth J. Haller (presently at Analytical Diffraction Services, Notre Dame, IN) for helpful crystallographic advice. L.F.D. would like to dedicate this paper to Professor Richard F. Fenske. The pioneering theoretical work of his group in developing and utilizing an approximate nonparameterized MO model has had and will continue to have a tremendous impact in providing new meaningful insight into the physical–chemical behavior of a wide variety of transition-metal clusters including the ones presented herein. I was most fortunate to have been associated with Professor Fenske during his 28 years at UW—Madison. He is a superb "critical, patient teacher" who taught me MO theory and greatly influenced my understanding of bonding–antibonding interactions in transition-metal clusters. Thanks, Dick, for making those 28 "short" years most memorable and enjoyable for me.

Supplementary Material Available: Thirteen tables of observed and calculated shifts at different temperatures for the proton resonances of $Co_3Cp'_3(\mu_3\text{-}S)_2$ (**1**) and $Co_3Cp_3(\mu_3\text{-}S)_2$ (**2**), positional parameters, anisotropic displacement coefficients, selected interatomic distances, and bond angles for the non-hydrogen atoms, and idealized coordinates and isotropic displacement coefficients for the hydrogen atoms of $Co_3Cp'_3(\mu_3\text{-}S)_2$ (**1**), $[Co_3Cp'_3(\mu_3\text{-}S)_2]^+[PF_6]^-$ ($\mathbf{1}^+[PF_6]^-$), and $[Co_3Cp'_3(\mu_3\text{-}S)_2]^{2+}[SbF_6]^-_2$ ($\mathbf{1}^{2+}[SbF_6]^-_2$) (18 pages); three tables of observed and calculated structure factor amplitudes for **1**, $\mathbf{1}^+[PF_6]^-$, and $\mathbf{1}^{2+}[SbF_6]^-_2$ (80 pages). Ordering information is given on any current masthead page.